ELSEVIER

Chemical Geology 243 (2007) 286–316

CHEMICAL GEOLOGY
INCLUDING
ISOTOPE GEOSCIENCE

www.elsevier.com/locate/chemgeo

Permian peralkaline, peraluminous and metaluminous A-type granites in the Panxi district, SW China: Their relationship to the Emeishan mantle plume

J. Gregory Shellnutt *, Mei-Fu Zhou

Department of Earth Sciences, The University of Hong Kong, Pokfulam Road, Hong Kong

Received 15 November 2006; received in revised form 15 May 2007; accepted 16 May 2007

Editor: R.L. Rudnick

Abstract

Numerous Permian granitic intrusions (plutons) in the Panxi region, SW China are spatially and temporally associated with the Emeishan large igneous province (ELIP). Granites from the 260 Ma Panzhihua and Taihe plutons are peralkaline (ASI=0.76–1.12; Na+K/Al=0.78–1.2) and have high Fe* values (0.92–0.99) with negative Eu anomalies (Eu/Eu*=0.22–0.98). Contrasted with the peralkaline plutons, syenites from the 260 Ma Woshui pluton are metaluminous (ASI=0.84–1.0; Na+K/Al=0.91–1.01) and have moderately high Fe* (0.79–0.81) and positive Eu-anomalies (Eu/Eu*=0.82–1.91). Both the peralkaline and metaluminous rocks have mantle isotopic signatures ($\varepsilon Nd_{(T)}$=+1.3–+3.2) and were derived from the ELIP mantle plume source. The peralkaline rocks were likely derived by fractional crystallization of the temporally, spatially and chemically associated layered mafic intrusions which host giant magmatic Fe-Ti-V oxide deposits. The metaluminous granitic rocks, although spatially related to the peralkaline granites and layered gabbros were likely generated by partial melting of underplated mafic rocks. Granites from the 251 Ma Ailanghe pluton are peraluminous (ASI=0.97–1.29) and have high Fe* (0.82–0.91) values and negative Eu-anomalies (Eu/Eu*=0.10–0.37). Their crustal isotopic signature ($\varepsilon Nd_{(T)}$=−5.7 to −6.7) indicates possible derivation from melting of Yangtze Block basement rocks. The Ailanghe pluton is contemporaneous with other A-type granites in the region, supporting the view that ELIP magmatism was sporadic for at least 9 million years. The coexistence of three chemically exclusive A-type granites in the ELIP suggests that a variety of A-type granites can be generated in the same tectonic setting.

Keywords: A-type; Peralkaline; Peraluminous; Metaluminous; Emeishan large igneous province; SW China

1. Introduction

Within-plate granite magmatism, although volumetrically small, is important for understanding the continued formation of the crust. Typically these granites form large batholiths of variable compositions (Pitcher, 1997; Smith et al., 1999). Generally these magmas are thought to form by either fractionation of basaltic magmas with or without crustal contamination (Loiselle and Wones, 1979; Turner et al., 1992; Smith et al., 1999; Anderson et al., 2003) or by melting of the crust (Collins et al., 1982; Whalen et al., 1987; Landenberger and Collins, 1996; Frost and Frost, 1997; King et al., 1997).

* Corresponding author. Tel.: +852 2859 1084.
E-mail address: jgshelln@hkusua.hku.hk (J.G. Shellnutt).

0009-2541/$ - see front matter © 2007 Elsevier B.V. All rights reserved.
doi:10.1016/j.chemgeo.2007.05.022

These granites are collectively termed as A-type which reflects their alkali- and iron-rich bulk composition and enriched rare earth element (REE) composition as well as their within-plate (anorogenic) tectonic setting.

The alumina saturation index (ASI=Al/(Ca-1.67P+Na+K) or Shand's index is a useful indicator to discriminate granites which have high Al_2O_3 content and thus a peraluminous (ASI>1.0) character from those which are metaluminous (Na+K<Al) and peralkaline (Na+K>Al) (Maniar and Piccoli, 1989; Frost et al., 2001). This subdivision of granitic rocks based on alumina allows for some interpretations regarding the petrogenesis of the granite in question. For example, peraluminous rocks are thought to be derived by melting of sedimentary sources (Chappell and White, 1974), although this may not represent every case (Miller, 1985; Turner et al., 1992; Frost et al., 2001). Nearly all peralkaline rocks have the characteristics of A-type granites whereas metaluminous and especially peraluminous granites are less likely to be so (Eby, 1990; King et al., 1997). Having peralkaline, peraluminous and metaluminous A-type granites in one region contemporaneous with the same igneous episode is rather special because their sources (i.e. mantle or crust) can be quite different from one another (Smith et al., 1999). Although all of these rocks may be considered A-type granites, they have different petrogenetic histories.

Large igneous provinces (LIPs) are most commonly known for their voluminous flood basalts and their economic potential. It is also known that LIPs may contain small volumes of felsic plutonic rocks which have A-type characteristics (Campbell and Hill, 1988; Coffin and Eldholm, 1994). The felsic plutonic rocks of many LIPs are largely left to cursory observation when compared to their mafic counterparts but they provide important insights into the origin and diversity of magmas produced during these voluminous magmatic events. In the Panxi region of SW China, peralkaline, peraluminous and metaluminous A-type granitic rocks are identified and all associated with the late Permian Emeishan large igneous province (ELIP). Within this region the peralkaline granitic rocks are always associated with layered mafic intrusions which host giant magmatic Fe-Ti-V oxide deposits. The metaluminous granitic rocks are alkalic and are located in the central portion of the Panxi region. At the southeastern corner of

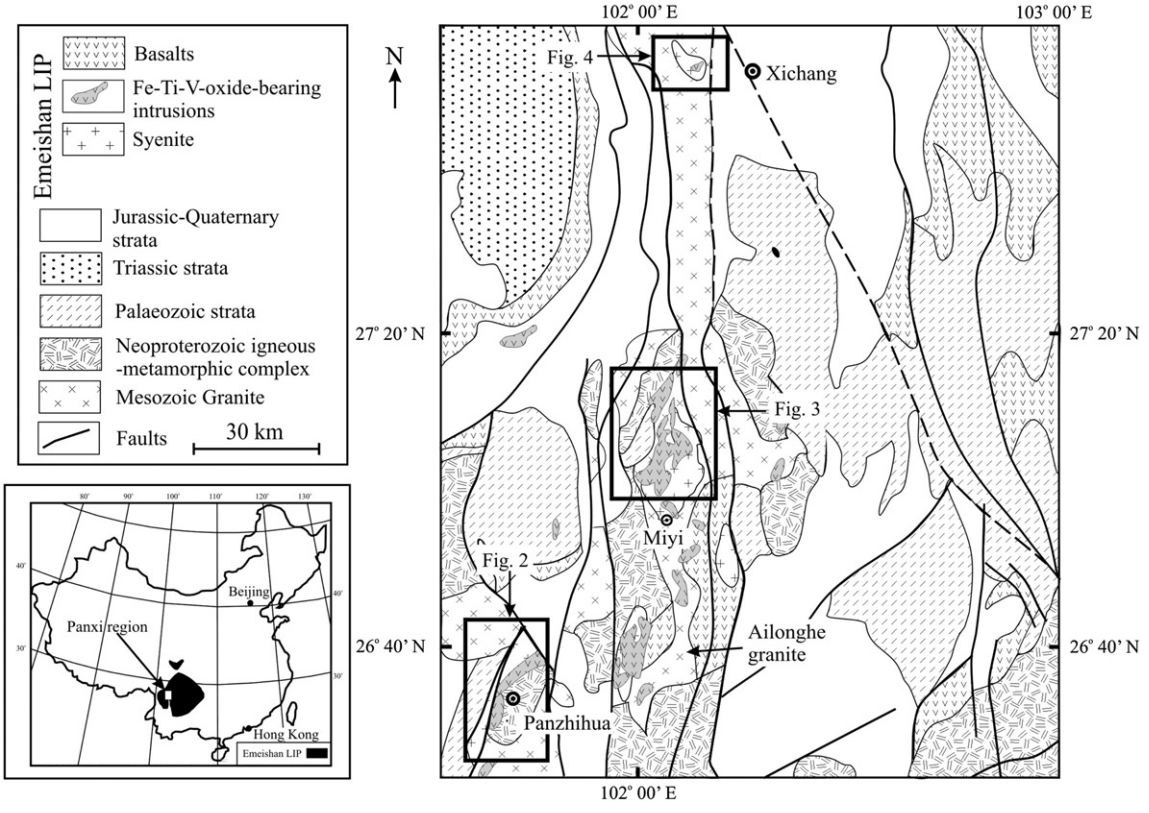

Fig. 1. Local geological map of the Panxi region, SW China, showing the distribution of mafic and felsic plutonic rocks. The Baima igneous complex is outlined in the boxed area (modified from Zhou et al., 2005).

the Panxi region is a calc-alkalic peraluminous A-type granitic intrusion which is spatially associated with Neoproterozoic basement rocks. The coexistence of three different A-type granites is unique as they could help understand the igneous processes required to form these mutually exclusive granitic rocks and their relationship to the formation of LIPs. This paper describes two peralkaline, one peraluminous and one metaluminous granitic intrusions. New major and trace elements, Sr–Nd isotopes and SHRIMP zircon U–Pb ages are presented to assess the petrogenetic significance of contemporaneous A-type granites in order to better understand their genetic relationship with the ELIP.

2. Geological background

2.1. Regional geology

Southwestern China comprises the western margin of the Yangtze Block to the east and the eastern most part of the Tibetan Plateau to the west (Fig. 1). The Yangtze Block consists of Mesoproterozoic granitic gneisses and metasedimentry rocks which have been intruded by Neoproterozoic (~800 Ma) granites (Zhou et al., 2002a). The origin of the Neoproterozoic granites remains controversial because Li et al. (1999) claim the granites were formed by crustal melting associated with a mantle plume whereas Zhou et al. (2002a) claim they formed within an active continental arc. The Neoproterozoic granites are overlain by a series of marine and terrestrial strata from the late Neoproterozoic (~600 Ma) to the Permian (Yan et al., 2003). The eastern part of the Tibetan Plateau is the Songpan-Ganze terrane, a late Triassic-early Jurassic thrust sequence composed of 10 km thick marine sediments known as the Xikang Group (Bruguier et al., 1997).

The largest, single geological feature of SW China is the middle-late Permian ELIP. It is located at the western edge of the Yangtze Block near the boundary with the Songpan-Ganze terrane (Fig. 1). The wedge shape of the ELIP is likely related to Mesozoic and Cenozoic faulting associated with the development of the Songpan-Ganze terrane and the Indo-Eurasian collision (Chung and Jahn, 1995). The ELIP covers an area of 0.3×10^6 km^2 of SW China and northern Vietnam and consists of flood basalts, spatially associated felsic plutons and layered

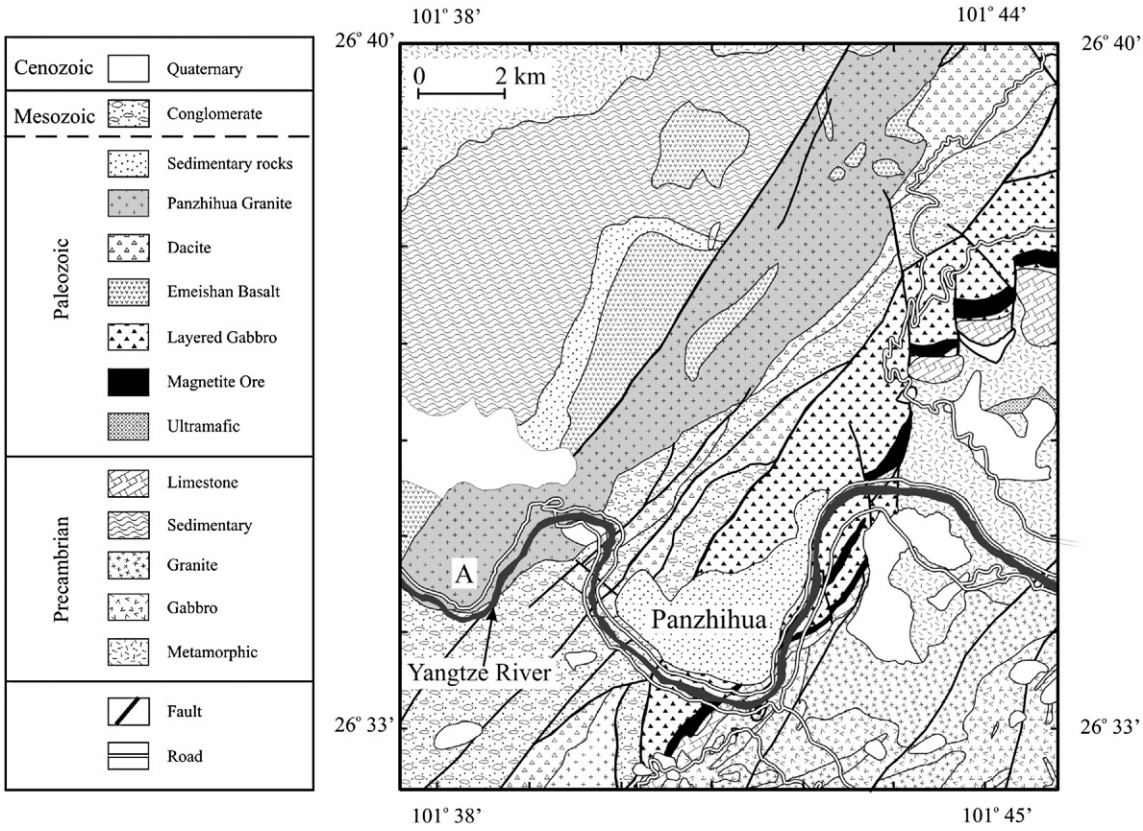

Fig. 2. Simplified geological map of Panzhihua. Samples were collected at site A across the width of the pluton (modified from Ma et al., 1999).

mafic-ultramafic intrusions, some of which host giant Fe-Ti-V oxide deposits (Zhong et al., 2002; Zhou et al., 2005). The volcanic succession is comprised of picrites, basaltic andesites and basalts which are subdivided into high- and low-Ti groups. The basalt piles range in thickness from 1.0 to 3.0 km in the western half and 0.2

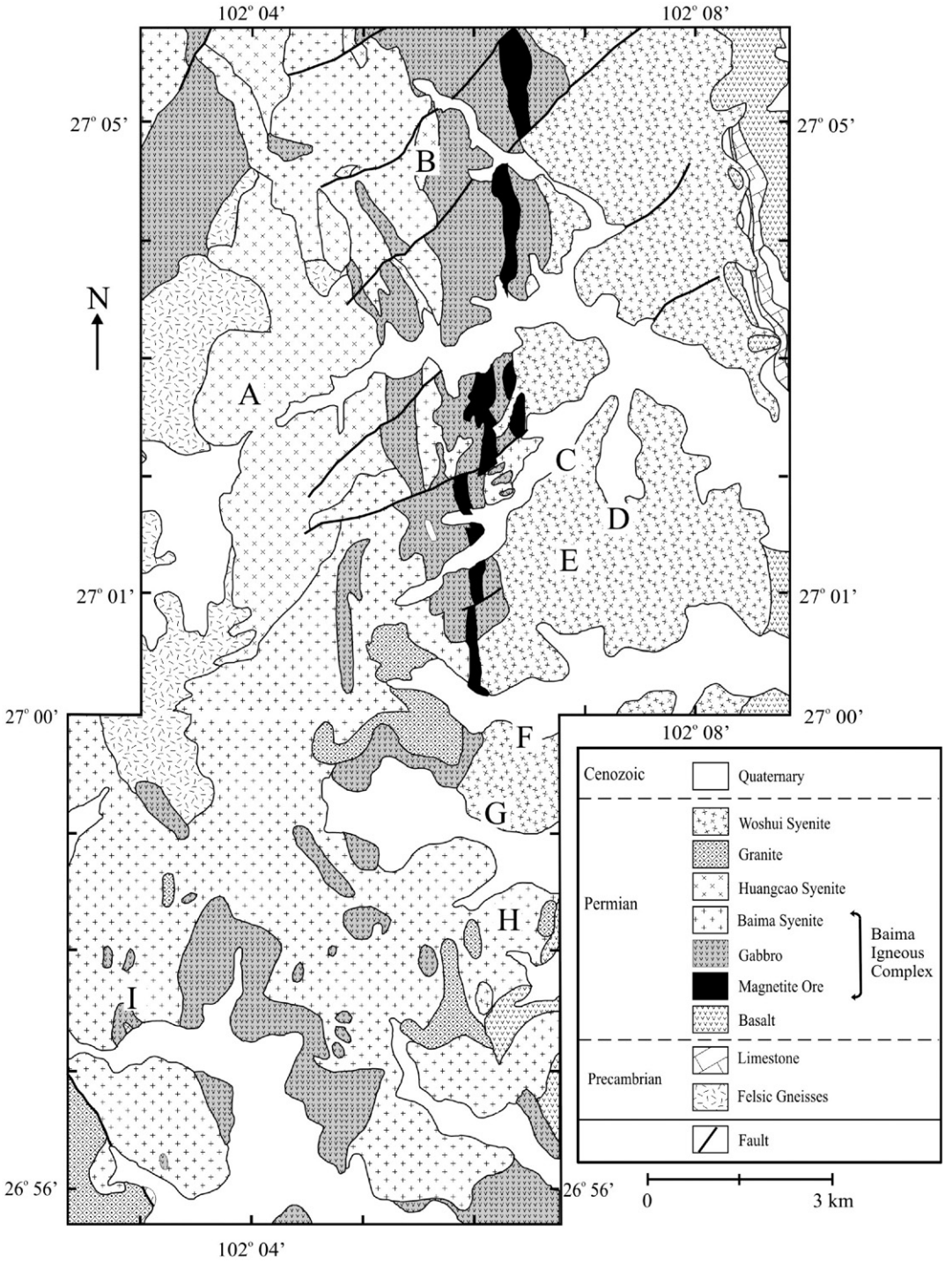

Fig. 3. Simplified geological map of the Baima igneous complex and the surrounding metaluminous syenites (modified from Wang et al., 1994; Xiong et al., 1996). The letters represent the sample locations.

to 2.6 km in the eastern half. The flood basalts and associated intrusions were likely produced by a mantle plume at ~260 Ma (Chung et al., 1998; Song et al., 2001; Xu et al., 2001; Zhou et al., 2002b, 2005; Guo et al., 2004).

The Panxi region, between Panzhihua and Xichang, of southern Sichuan province (Fig. 1) hosts a diverse assemblage of within-plate granitic rocks. Many of these plutons are associated with layered gabbroic intrusions which host magmatic Fe-Ti-V oxide deposits (Zhong et al., 2002; Zhou et al., 2005). Many deposits, such as those in the Panzhihua, Baima, Taihe, Hongge and Xinjie intrusions, are either being developed for mining or are currently mined for Fe, Ti and V (Zhong et al., 2002; Zhou et al., 2005; Shellnutt et al., 2005).

2.2. Distribution of felsic plutons in the Panxi region

Numerous felsic plutons in the Panxi region are distributed along a narrow belt ~50 km wide and 200 km long. The axis of the plutonic belt changes from northeast-southwest to north-south near the town of Miyi in the central part of the Panxi region (Fig. 1). The most common types of felsic plutonic rocks are syenite and granite. Peralkaline granitic and syenitic intrusions are most commonly associated with oxide ore-bearing layered mafic-ultramafic intrusions, e.g., the Panzhihua, Baima and Taihe intrusions (Zhou et al., 2005; Shellnutt et al., 2005; Shellnutt and Zhou, 2006a) (Figs. 2–4). The close proximity of the peralkaline plutons to the Fe-Ti-V deposits has led to speculation that they are directly associated with the formation of the deposits (Yang et al., 1997). In addition to the peralkaline plutons, there are metaluminous syenites, such as the Woshui pluton and fayalite bearing Huangcao pluton (Fig. 3), associated with the Baima igneous complex (BIC). It is common to find 10–20 cm wide felsic dykelets intruding the mafic lower cumulate zone of the BIC. These dykelets are thought to originate from the Woshui pluton due to their textural similarities and proximity to the lower cumulate zone (Fig. 3). The Huangcao syenite sporadically intrudes the upper gabbro zone and syenite of the BIC however the bulk of the pluton is to the west of the BIC and the contacts are unexposed. In a few locations, notably Panzhihua and Hongge, peraluminous plutons (e.g. the Ailanghe pluton) are located within a few kilometers of the ore deposits (Fig. 1).

3. Petrography

3.1. Panzhihua granitic intrusion

The granites are granular and coarse grained and consists primarily of alkali feldspar, quartz and ferrorichterite. Accessory minerals include apatite and zircon. The alkali feldspar is subhedral, rectangular to angular in shape and comprised 65–70% of the mode. The alkali feldspar crystals are usually 1.5 cm or less in length and have patchy exsolution lamellae likely caused by the ubiquitous alteration of the feldspars to

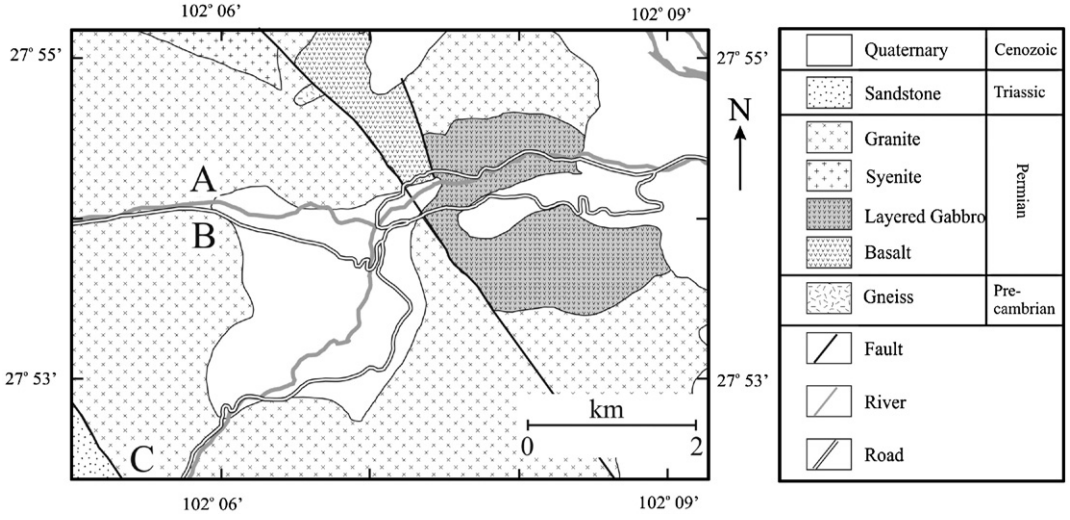

Fig. 4. Simplified geological map of the Taihe granitic pluton and associated layered gabbroic intrusion (modified from Wang et al., 1993). Letters represent the sampling localities.

Table 1
SHRIMP zircon analytical data of the Woshui syenite

Spot	U (ppm)	Th (ppm)	$^{206}Pb_c$ (%)	$^{206}Pb^*$ (ppm)	(1) $^{206}Pb/^{238}U$ Age		(2) $^{206}Pb/^{238}U$ Age		(3) $^{206}Pb/^{238}U$ Age		(1) $^{208}Pb/^{232}Th$ Age	
GS05-065.1	102	83	1.55	3.77	267.1	±4.5	268.2	±4.4	266.0	±5.2	275	±13
GS05-065.2	98	83	1.87	3.59	263.3	±4.6	264.1	±4.4	264.0	±5.2	259	±14
GS05-065.3	80	84	3.24	2.88	257.6	±4.9	260.5	±4.7	258.7	±5.8	252	±16
GS05-065.4	185	28	1.30	6.59	258.7	±3.9	260.2	±3.9	259.8	±4.0	214	±41
GS05-065.5	412	312	0.82	14.6	257.8	±3.5	258.6	±3.6	258.4	±4.0	253.2	±6.3
GS05-065.6	183	89	1.07	6.47	256.6	±3.9	257.6	±3.8	257.0	±4.2	252	±14
GS05-065.7	103	106	2.72	3.60	249.3	±7.0	252.3	±6.9	253.3	±8.6	228	±16
GS05-065.8	286	561	0.84	10.3	262.3	±3.7	263.0	±3.7	263.4	±5.7	259.8	±4.9
GS05-065.9	180	185	1.08	6.42	259.7	±3.9	260.8	±3.9	257.5	±4.8	271.2	±7.8
GS05-065.10	135	105	0.51	4.85	263.5	±4.1	262.6	±4.1	263.0	±4.7	267.2	±7.0
GS05-065.11	49	33	2.34	1.75	255.6	±5.7	257.4	±5.1	256.2	±5.9	250	±28
GS05-065.12	45	30	3.02	1.61	257.5	±5.5	257.3	±5.3	256.6	±6.2	265	±23
GS05-065.13	67	53	2.42	2.42	261.1	±5.0	262.3	±4.8	262.4	±5.6	252	±18
GS05-065.14	92	90	1.49	3.34	262.8	±4.6	262.9	±4.5	263.1	±5.4	261	±13
GS05-065.15	126	149	1.53	4.53	260.4	±4.2	261.3	±4.1	261.9	±5.2	253.5	±8.8

Errors are 1—sigma; Pb_c and Pb* indicate the common and radiogenic portions, respectively.
Error in Standard calibration was 0.64% (not included in above errors but required when comparing data from different mounts).
(1) Common Pb corrected using measured ^{204}Pb.
(2) Common Pb corrected by assuming $^{206}Pb/^{238}U$–$^{207}Pb/^{235}U$ age-concordance.
(3) Common Pb corrected by assuming $^{206}Pb/^{238}U$–$^{208}Pb/^{232}Th$ age-concordance.
Sample collected at 27°01′41″ N, 102°06′27″ E.

clay minerals. Quartz (≤1 mm) comprises ~20–25% of the mode and is rounded to sub-rounded and interstitial to the alkali feldspar. Most often the quartz has formed an interlocking network however in some cases it appears to embay the alkali feldspar. Interstitial to the feldspar and quartz is ferrorichterite comprising ~10–15% of the mode. The ferrorichterite is euhedral to subhedral and has formed between the feldspar and quartz crystals causing an angular appearance. Generally the eastern portion of the intrusion contains slightly more amphibole than the western portion. Accessory zircon and apatite (≪1%) are occasionally found within the ferrorichterite. Oxide minerals were either absent or have extremely low quantities.

3.2. Taihe granitic intrusion

Granites in Taihe are texturally and mineralogically similar to those of the Panzhihua granitic intrusion. They are granular and coarse grained and consist mostly of feldspar, quartz and amphibole. The alkali feldspar is euhedral to subhedral with fine, linear exsolution, a marked difference from the Panzhihua granite. The crystals are typically 1–2 cm in size and comprise ~65–70% of bulk mineralogy. The quartz is ≤0.2 cm and is rounded and interstitial to the alkali feldspar and often forms an interlocking network which comprise 20–25% of the mode. The only major mafic mineral, ferrorichterite, is angular and interstitial to feldspars and contains a small amount of apatite. The ferrocrichterite is partially altered to reibeckite/arfvedsonite and in some cases a translucent red-brown mineral likely to be hematite. Small amounts (<1%) of subhedral aegirine and anhedral zircon are also present.

3.3. Woshui syenitic intrusion

The syenites consist of alkali feldspar which has serrated boundaries and angular to sub-round shapes. The alkali feldspar varies in size from 2 cm to <0.1 cm and comprises ~80% of the mineral mode and shows perthite, microcline perthite and microperthite exsolution textures. Fe-rich amphibole (~15%) is the principle mafic mineral interstitial to the feldspar and often forms clusters with Fe-Ti oxides. The angular shape and size (≤1 cm) of the amphibole are determined by cleavage planes and the space available to crystallize. Commonly within the cluster of amphibole are small (≤0.1 cm), irregularly shaped Fe-Ti oxides (~2%) which host small euhedral apatite crystals (<1%). There is a small amount (<1%) of euhedral zircon, biotite and clinopyroxene as well.

Table 2
Whole rock geochemistry of the Permian Panxi granites

Sample	GS03-061	GS04-087	GS04-088	GS04-089	GS04-090	GS04-091	GS04-092	GS04-093	GS04-094	GS04-095	GS04-096
Location	Ailanghe	Ailanghe	Ailanghe	Ailanghe	Ailanghe	Ailanghe	Ailanghe	Ailanghe	Ailanghe	Ailanghe	Ailanghe
SiO_2 (wt.%)	76.80	76.59	74.57	76.05	76.08	75.53	77.16	73.20	78.73	76.69	76.26
TiO_2	0.17	0.14	0.12	0.16	0.16	0.10	0.15	0.22	0.12	0.13	0.16
Al_2O_3	12.06	12.32	13.59	12.67	12.75	12.31	11.16	13.33	11.02	11.70	11.56
Fe_2O_3t	1.17	1.09	1.30	1.09	1.20	1.11	1.58	1.51	1.62	1.45	2.18
MnO	0.02	0.01	0.01	0.01	0.02	0.01	0.01	0.02	0.02	0.02	0.03
MgO	0.23	0.13	0.12	0.20	0.17	0.15	0.18	0.14	0.22	0.17	0.30
CaO	1.13	0.25	0.44	0.15	0.40	0.56	0.26	2.28	0.34	0.42	0.37
Na_2O	2.03	2.56	2.88	2.19	2.60	2.99	2.44	2.81	2.19	2.68	2.33
K_2O	5.35	4.79	4.51	4.95	5.06	4.90	4.03	4.59	4.00	4.63	4.18
P_2O_5	0.00	0.00	0.00	0.00	0.00	0.00	0.01	0.03	0.00	0.00	0.00
LOI	0.98	1.22	1.03	1.27	1.20	1.30	1.53	1.12	0.96	0.86	1.25
Total	99.93	99.09	98.56	98.73	99.64	98.97	98.52	99.24	99.23	98.75	98.64
ANCK	1.08	1.25	1.31	1.37	1.22	1.09	1.26	0.97	1.29	1.15	1.28
Na+K/Al	0.76	0.76	0.71	0.71	0.77	0.83	0.75	0.72	0.72	0.81	0.72
K_2O/Na_2O	2.63	1.87	1.57	2.26	1.94	1.64	1.66	1.63	1.82	1.73	1.79
Fe*	0.82	0.88	0.91	0.83	0.86	0.87	0.89	0.91	0.87	0.88	0.87
Sc (ppm)		13	14	12	10	16	15	15	13	13	11
V		3	3	5	6	3	5	13	5	4	5
Cr		1	1	3	3	1	4	5	2	3	2
Co		0	1	0	1	0	1	1	1	1	1
Ni		1	2	3	3	2	3	5	2	3	2
Cu		0	0	1	1	1	2	2	0	1	0
Zn		15	20	12	17	15	16	9	38	18	18
Ga		15.1	17.0	13.5	15.5	12.8	12.2	13.6	15.3	14.4	16.0
Rb		256	271	258	259	223	174	164	190	196	185
Sr		38	41	58	62	46	48	405	48	48	43
Y		47	78	22	35	30	18	41	33	30	41
Zr		170	149	142	161	124	147	201	154	154	181
Nb		36	39	21	30	31	34	23	28	31	37
Cs		3.3	5.0	6.0	5.5	2.3	2.0	1.4	2.7	2.5	2.4
Ba		123	120	288	261	169	134	673	136	136	143
La		62.2	79.2	23.8	82.9	22.5	28.0	53.9	90.0	72.8	79.8
Ce		64.7	106.3	33.4	109.4	28.7	54.8	105.1	172.5	139.7	153.4
Pr		12.8	16.8	4.5	13.4	4.5	5.5	12.4	16.3	14.3	15.8
Nd		43.7	59.4	13.6	43.3	16.4	17.7	43.3	54.8	45.8	51.1
Sm		8.9	13.1	2.4	7.4	3.3	3.0	8.9	9.1	8.2	9.0
Eu		0.4	0.5	0.3	0.6	0.2	0.2	0.7	0.4	0.4	0.4
Gd		9.2	14.2	3.4	9.7	4.0	4.2	9.2	10.9	9.5	10.3
Tb		1.4	2.3	0.6	1.1	0.7	0.6	1.4	1.3	1.2	1.4
Dy		8.6	14.2	3.5	6	4.7	3.4	8.5	6.7	6.4	8.2
Ho		1.9	2.9	0.8	1.3	1.1	0.7	1.7	1.3	1.2	1.6
Er		6.3	8.9	2.5	4.3	3.6	2.4	5.4	4.5	4.2	5.3
Tm		1.0	1.4	0.4	0.6	0.6	0.4	0.8	0.7	0.6	0.8
Yb		6.7	9.1	2.7	3.9	3.9	2.6	5.4	4.3	3.9	5.4
Lu		1	1.4	0.4	0.6	0.6	0.4	0.7	0.6	0.6	0.9
Hf		7.1	6.7	5.3	6.6	5.9	5.8	6.6	6.5	6.7	7.6
Ta		4.2	4.3	3.4	3.3	4.8	3.3	2.1	2.4	3.0	3.7
Th		43.4	40.6	61.0	61.9	37.5	41.7	21.6	40.0	40.6	46.6
U		13.6	11.8	8.8	15.6	5.9	6.2	5.8	7.3	7.4	8.5
Eu/Eu*		0.12	0.10	0.29	0.23	0.17	0.21	0.24	0.11	0.13	0.13
$(La/Sm)_N$		4.5	3.9	6.5	7.2	4.5	6.0	3.9	6.4	5.7	5.7
$(La/Yb)_N$		6.7	6.2	6.4	15.1	4.2	7.8	7.2	15.1	13.3	10.6

ANCK = molar Al/Na + Ca + K; Fe = FeO/MgO, FeO = 0.8998*Fe_2O_3t; Eu/Eu* = 2*$Eu_N/[Sm_N+Gd_N]$.

GS04-097	GS04-054	GS04-055	GS04-056	GS04-057	GS04-058	GS04-059	GS04-061A	GS04-062	GS04-063A	GS04-065
Ailanghe	Taihe	Taihe	Taihe	Taihe	Taihe	Taihe	Taihe	Taihe	Taihe	Taihe
74.69	70.88	72.40	74.38	70.78	69.80	71.88	72.87	71.69	72.26	71.75
0.19	0.48	0.32	0.23	0.44	0.65	0.44	0.30	0.35	0.38	0.31
12.82	11.62	11.64	11.64	11.45	11.21	10.94	11.57	11.28	10.55	11.17
1.55	5.89	4.78	3.53	5.80	6.89	5.83	4.21	5.56	5.71	5.62
0.02	0.17	0.14	0.10	0.16	0.20	0.14	0.12	0.14	0.14	0.15
0.25	0.13	0.13	0.07	0.11	0.13	0.11	0.10	0.10	0.10	0.13
0.61	0.69	0.67	0.40	0.64	0.75	0.54	0.53	0.45	0.55	0.58
2.62	4.90	4.71	4.45	4.78	5.18	4.74	4.66	4.70	4.55	4.74
4.89	4.83	4.85	4.90	4.78	4.39	4.72	4.95	4.80	4.57	4.61
0.03	0.03	0.03	0.02	0.03	0.03	0.02	0.02	0.02	0.02	0.03
1.12	0.25	0.32	0.26	0.16	0.65	0.45	0.65	0.57	0.39	0.39
98.79	99.87	99.98	99.98	99.14	99.88	99.81	99.98	99.66	99.23	99.47
1.20	0.80	0.82	0.87	0.81	0.77	0.79	0.83	0.82	0.79	0.81
0.75	1.14	1.12	1.08	1.14	1.18	1.18	1.13	1.15	1.18	1.14
1.87	0.99	1.03	1.10	1.00	0.85	1.00	1.06	1.02	1.00	0.97
0.85	0.98	0.97	0.98	0.98	0.98	0.98	0.98	0.98	0.98	0.98
11	8	8	7	8	7	7	8	7	7	7
9	3	2	1	2	3	2	2	4	3	2
3	2	4	3	2	7	4	2	3	5	3
1	1	1	0	1	1	0	1	1	1	1
2	4	6	6	4	7	6	4	4	38	5
1	6	89	110	8	55	14	16	54	28	11
20	219	204	306	217	283	219	236	312	245	235
13.4	35.7	35.3	36.0	37.1	36.3	36.0	38.0	40.3	35.5	35.4
177	128	130	141	140	124	141	139	140	137	142
99	15	20	13	17	19	14	12	14	13	17
16	95	82	110	103	98	82	152	245	126	88
127	585	710	1400	675	421	608	545	542	563	595
18	96	99	97	108	120	105	112	111	115	103
2.8	0.4	0.4	0.6	0.4	0.6	0.5	0.5	0.5	0.5	0.5
460	326	344	290	369	382	295	198	187	180	315
52.9	108.1	99.1	103.8	148.6	112.8	103.1	465.8	607.2	189.1	122.8
91.2	272.8	198.3	208.5	354.8	305.5	253.9	375.4	662.6	332.2	305.4
9.4	26.8	24.8	24.5	35.0	28.0	25.4	94.2	104.2	44.8	29.1
30.7	102.8	94.8	90.8	132.8	105.5	93.1	345.4	381.4	174.6	109.1
4.9	20.0	18.3	17.6	25.2	20.6	18.3	62.6	66.5	33.4	20.2
0.7	3.2	2.8	2.7	3.9	3.2	2.8	8.6	9.3	5	3.0
6.2	17.5	15.5	16.2	21.1	17.8	15.8	44.2	52.0	29.5	17.3
0.7	3.0	2.6	2.9	3.5	3.0	2.7	6.8	7.5	4.9	2.7
3.4	17.8	15.9	19.3	20.7	18.8	16.0	35.0	38.6	27.7	16.4
0.6	3.6	3.3	4.2	4.1	3.8	3.3	6.2	6.7	5.2	3.4
2.0	10.7	9.9	13.0	12.0	11.0	9.8	16.6	17.4	14.5	10.6
0.3	1.5	1.5	1.8	1.7	1.6	1.4	2.2	2.2	2.0	1.6
1.7	10.1	9.7	11.2	10.9	10.4	9.4	14	14.1	12.8	11.0
0.2	1.5	1.4	1.5	1.6	1.5	1.4	2.1	2.1	1.9	1.7
4.6	16.0	19.0	36.4	18.7	11.6	16.4	15.8	15.3	15.7	16.2
1.7	5.6	6.2	6.6	6.8	6.4	6.8	7.5	6.4	7.1	7.1
33.5	16.0	19.3	23.0	20.8	17.4	19.5	17.1	30.4	20.0	17.5
5.4	3.6	4.5	7.4	4.3	3.2	4.1	4.1	4.3	4.1	3.8
0.37	0.50	0.49	0.49	0.50	0.50	0.48	0.48	0.47	0.48	0.48
7.0	3.5	3.5	3.8	3.8	3.5	3.6	4.8	5.9	3.7	3.9
21.8	7.7	7.3	6.7	9.8	7.8	7.9	23.9	31.0	10.6	8.0

(continued on next page)

Table 2 (*continued*)

Sample	GS04-066	GS04-067	GS04-069	GS04-147	GS04-148	GS04-149	GS04-150	GS04-151	GS04-152	GS04-153
Location	Taihe	Taihe	Taihe	Taihe	Taihe	Taihe	Taihe	Taihe	Taihe	Taihe
SiO_2 (wt.%)	72.85	70.21	71.48	75.01	73.09	71.74	74.11	73.00	70.64	73.04
TiO_2	0.37	0.52	0.38	0.23	0.40	0.51	0.34	0.27	0.57	0.40
Al_2O_3	10.35	10.85	10.88	11.95	10.26	10.62	9.60	10.62	10.68	11.17
Fe_2O_3t	5.20	6.95	5.58	2.44	4.97	5.87	6.62	5.71	6.73	4.59
MnO	0.14	0.18	0.14	0.06	0.11	0.15	0.12	0.09	0.20	0.13
MgO	0.09	0.11	0.09	0.17	0.15	0.14	0.21	0.24	0.18	0.19
CaO	0.52	0.64	0.60	0.47	0.43	0.48	0.39	0.38	0.69	0.45
Na_2O	4.45	4.93	4.75	3.77	4.40	4.70	3.53	4.09	4.41	4.34
K_2O	4.29	4.46	4.56	4.99	4.41	4.59	4.44	4.75	4.39	4.61
P_2O_5	0.02	0.02	0.02	0.03	0.02	0.02	0.02	0.02	0.04	0.03
LOI	0.36	0.28	0.32	0.41	0.55	0.40	0.42	0.55	0.41	0.43
Total	98.63	99.14	98.82	99.54	98.79	99.22	99.78	99.72	98.93	99.39
ANCK	0.80	0.77	0.79	0.96	0.80	0.78	0.85	0.85	0.81	0.86
Na+K/Al	1.16	1.19	1.17	0.97	1.17	1.19	1.10	1.12	1.12	1.09
K_2O/Na_2O	0.96	0.90	0.96	1.32	1.00	0.98	1.26	1.16	1.00	1.06
Fe*	0.98	0.98	0.98	0.93	0.97	0.97	0.97	0.96	0.97	0.96
Sc (ppm)	8	8	8	12	15	18	15	13	14	15
V	2	2	2	3	2	1	1	2	2	2
Cr	7	3	5	2	1	1	0	1	3	1
Co	1	1	0	1	0	0	0	0	1	0
Ni	10	5	5	2	1	2	1	1	2	1
Cu	21	9	69	2	3	4	2	4	7	4
Zn	212	270	225	108	164	184	214	209	231	176
Ga	34.1	37.1	34.0	21.1	30.9	34.2	33.0	30.6	33.7	30.0
Rb	137	144	136	150	107	108	157	139	99	100
Sr	14	19	17	21	8	9	6	8	11	8
Y	83	112	77	45	97	113	77	74	89	91
Zr	750	496	775	445	590	774	708	688	651	702
Nb	106	120	88	53	86	108	88	97	103	115
Cs	0.5	0.8	0.4	0.5	1.0	1.0	0.4	0.4	0.7	0.4
Ba	302	308	267	244	105	107	81	155	249	240
La	101.4	164.8	96.1	140.4	100.8	137	145.2	122.4	125.2	112.1
Ce	286.3	386.0	236.3	266.1	188.9	271.4	236	243	265.6	235.9
Pr	24.4	40.4	24.1	25.4	25.4	30.4	30.6	26.4	30.0	28.7
Nd	92.4	152.6	90.8	88.0	96.7	110.5	104.4	100.1	112.1	112.6
Sm	18.3	29.0	17.3	14.4	21.0	22.0	19.1	18.3	22.6	21.5
Eu	2.8	4.3	2.6	1.1	2.7	2.6	2.3	2.4	2.9	2.9
Gd	15.8	23.7	14.8	16.7	20.7	23.3	19.5	18.8	22.3	21.8
Tb	2.7	4.0	2.5	2.1	3.4	3.6	2.8	2.8	3.3	3.4
Dy	16.2	22.9	14.9	10.6	20.0	21.8	15.8	15.6	19.0	18.9
Ho	3.3	4.5	3.1	2.0	4.1	4.5	3.1	3.2	3.8	3.8
Er	10.2	13.0	9.2	6.5	12.1	14.4	10.2	10.4	11.7	11.9
Tm	1.5	1.9	1.4	0.9	1.7	2.0	1.5	1.5	1.6	1.7
Yb	10.2	12.6	9.2	5.4	10.3	12.4	10.4	9.3	10.7	10.1
Lu	1.5	1.9	1.4	0.8	1.5	1.9	1.6	1.4	1.7	1.5
Hf	20.6	14.2	21.0	11	17.7	24.8	19.9	20.5	19.3	19.1
Ta	7.2	7.3	5.9	2.6	6.0	7.8	6.5	6.8	7.0	8.1
Th	21.5	20.5	16.5	16.2	13.8	18.9	14.5	16.9	16.8	20.8
U	4.5	3.8	4.5	2.6	3.4	4.6	3.9	4.1	3.9	4.4
Eu/Eu*	0.49	0.48	0.49	0.22	0.39	0.35	0.36	0.39	0.39	0.40
$(La/Sm)_N$	3.6	3.7	3.6	6.3	3.1	4.0	4.9	4.3	3.6	3.4
$(La/Yb)_N$	7.1	9.4	7.5	18.6	7.0	7.9	10.0	9.4	8.4	7.9

GS04-155	GS04-156	GS04-157	GS04-158	GS03-005	GS03-007	GS03-008	GS03-009	GS03-010	GS03-011	GS03-012
Taihe	Taihe	Taihe	Taihe	Panzhihua	Panzhihua	Panzhihua	Panzhihua	Panzhihua	Panzhihua	Panzhihua
70.91	71.52	75.08	73.15	71.57	70.67	68.70	70.75	71.45	70.22	70.22
0.38	0.40	0.23	0.36	0.29	0.25	0.47	0.47	0.39	0.48	0.54
11.38	11.31	12.02	11.55	13.12	11.30	11.83	10.92	11.62	10.96	11.81
5.36	5.12	2.49	4.90	2.56	6.32	6.82	6.42	5.09	6.53	6.15
0.16	0.15	0.06	0.14	0.03	0.17	0.17	0.15	0.14	0.16	0.16
0.20	0.18	0.08	0.08	0.15	0.16	0.09	0.14	0.06	0.09	0.05
0.69	0.65	0.45	0.58	0.81	0.66	0.59	0.85	0.59	0.67	0.21
4.81	4.51	3.55	4.38	4.74	5.16	4.92	5.12	5.18	5.14	5.01
4.65	4.37	4.99	4.78	4.33	4.17	4.22	3.87	4.44	4.37	4.60
0.03	0.03	−0.01	0.00	0.04	0.03	0.02	0.03	0.03	0.01	0.00
0.41	0.37	0.23	0.26	1.55	0.52	1.62	1.15	0.92	1.04	1.19
98.98	98.62	99.18	100.19	99.18	99.42	99.44	99.86	99.89	99.67	99.93
0.80	0.85	1.00	0.86	0.94	0.80	0.86	0.77	0.81	0.76	0.87
1.14	1.08	0.94	1.07	0.95	1.15	1.07	1.16	1.15	1.20	1.12
0.97	0.97	1.41	1.09	0.91	0.81	0.86	0.76	0.86	0.85	0.92
0.96	0.96	0.96	0.98	0.94	0.97	0.99	0.98	0.99	0.98	0.99
18	12	17	18	8	12	11	13	14	14	13
3	2	3	3	10	1	2	2	1	1	1
3	5	3	4	2	17	2	2	9	3	2
1	1	1	1	2	1	1	0	0	0	0
2	3	2	2	4	9	3	1	6	5	1
5	4	3	4	29	4	5	5	5	6	5
234	190	197	196	57	264	263	258	267	282	238
34.3	32.3	34.0	32.1	24.1	35.7	40.1	39.1	40.2	39.7	39.4
124	119	128	123	56	78	92	77	93	90	93
17	14	12	14	65	24	16	25	42	31	13
92	94	83	96	56	68	76	78	76	80	69
892	733	685	1182	807	771	972	946	1057	1022	892
108	103	112	112	63	74	87	83	91	91	78
0.7	0.6	0.6	0.7	0.2	0.2	0.3	0.2	0.3	0.2	0.3
397	356	387	305	371	417	392	479	555	496	355
131.9	119.6	121.8	131.8	97.3	74.6	79.2	92.9	107.1	107.7	80.0
267.8	256.3	291.7	251.3	237.6	146.1	185.8	235.4	276.6	270.0	205.4
30.2	29.4	30.9	31.0	20.8	19.1	21.4	23.9	26.5	27.8	21.2
113.5	108.9	104.5	113.7	75.1	73.2	81.4	93.7	103.2	108.6	82.9
22.8	21.2	21.8	22.6	13.8	14.9	17.2	19.2	20.6	21.5	17.2
3.1	3.1	3.2	3.3	2.5	3.3	3.8	4.0	4.2	4.7	4.1
21.8	20.8	21.1	22.6	11.5	13.3	15.4	17.2	18.2	18.9	15.4
3.3	3.2	3.4	3.4	1.8	2.2	2.5	2.7	2.8	2.9	2.4
19.1	18.9	18.5	19.9	10.6	13.5	15.3	15.8	15.7	16.6	14.1
3.9	3.8	3.7	4.1	2.2	2.7	3.0	3.1	3.0	3.2	2.8
12.5	12.6	11.6	13.0	6.2	7.6	8.5	8.8	8.6	9.0	7.7
1.8	1.8	1.6	1.9	0.9	1.1	1.2	1.2	1.2	1.2	1.1
11.1	11.5	10.2	11.8	5.4	6.7	7.5	7.4	7.4	7.7	6.7
1.7	1.7	1.5	1.7	0.8	1	1.1	1.1	1	1.1	1.0
24.1	25.0	19.3	29.3	16.9	14.9	18.5	18.4	20.1	20.2	17.4
6.6	7.6	7.6	8.3	4.8	4.8	5.6	5.6	6.0	6.3	5.0
18.1	17.8	23.5	20.2	19.1	10.9	13.4	13.7	15.5	15.4	11.6
4.9	4.8	4.4	5.7	3.0	2.2	2.6	2.7	2.7	3.1	3.0
0.42	0.45	0.45	0.44	0.58	0.70	0.70	0.65	0.64	0.69	0.75
3.7	3.6	3.6	3.8	4.6	3.2	3.0	3.1	3.3	3.2	3.0
8.6	7.5	8.6	8.0	12.9	8.0	7.6	9.0	10.4	10.1	8.6

(continued on next page)

Table 2 (*continued*)

Sample	GS03-013	GS03-014	GS03-015	GS03-016	GS03-017	GS03-018	GS03-019	GS03-020	GS03-021	GS03-022
Location	Panzhihua	Panzhihua	Panzhihua	Panzhihua	Panzhihua	Panzhihua	Panzhihua	Panzhihua	Panzhihua	Panzhihua
SiO_2 (wt.%)	68.71	69.93	71.72	70.08	71.01	71.34	72.48	74.94	69.99	65.36
TiO_2	0.50	0.56	0.45	0.49	0.54	0.47	0.49	0.48	0.51	0.79
Al_2O_3	10.98	11.07	10.87	11.19	10.65	10.93	10.74	11.49	11.42	13.03
Fe_2O_3t	6.82	6.11	5.58	5.70	7.20	7.14	8.28	4.89	7.04	7.24
MnO	0.18	0.13	0.11	0.15	0.18	0.12	0.06	0.02	0.17	0.19
MgO	0.17	0.45	0.24	0.42	0.06	0.09	0.05	0.06	0.35	0.17
CaO	0.62	0.71	0.59	0.99	0.06	0.09	0.00	0.02	0.77	1.01
Na_2O	4.64	4.57	4.66	5.03	4.82	4.67	3.80	3.22	4.98	5.80
K_2O	4.03	4.31	4.30	4.24	3.88	3.83	3.81	4.56	4.28	4.29
P_2O_5	0.03	0.03	0.03	0.00	0.00	0.00	0.00	0.00	0.00	0.05
LOI	2.91	1.36	1.13	1.54	1.46	1.10	1.38	1.04	0.93	1.63
Total	99.59	99.24	99.68	99.84	99.86	99.78	101.07	100.72	100.44	99.57
ANCK	0.84	0.82	0.81	0.76	0.87	0.91	1.04	1.12	0.80	0.81
Na+K/Al	1.09	1.10	1.13	1.15	1.14	1.08	0.97	0.89	1.12	1.09
K_2O/Na_2O	0.87	0.94	0.92	0.84	0.81	0.82	1.00	1.41	0.86	0.74
Fe*	0.97	0.92	0.95	0.92	0.99	0.99	0.99	0.99	0.95	0.97
Sc (ppm)	12	12	12	11	11	12	12	9	12	13
V	2	2	1	2	2	2	3	3	1	2
Cr	2	2	3	3	6	3	4	6	7	3
Co	0	0	0	0	0	0	0	0	0	1
Ni	1	1	1	1	43	1	3	2	11	3
Cu	4	4	3	4	5	4	4	4	6	9
Zn	247	260	235	264	298	348	263	172	301	232
Ga	38.2	38.0	39.7	38.9	40.6	41.4	39.7	42.9	40.2	37.6
Rb	86	98	95	99	75	85	87	131	105	91
Sr	39	32	33	36	10	13	8	11	27	43
Y	80	76	90	76	89	110	129	107	76	60
Zr	919	947	1155	977	1050	1400	1820	1410	942	738
Nb	83	85	95	93	101	125	145	126	85	85
Cs	0.1	0.3	0.3	0.3	0.1	0.2	0.1	0.3	0.3	0.4
Ba	455	207	538	508	342	301	234	170	494	618
La	84.9	88.4	107.2	98.7	94.4	127.4	75.7	114.0	100.1	84.3
Ce	214.5	231.6	279.5	256.2	248.1	341.6	344.2	312	258.4	171.4
Pr	21.6	23.3	28	25.7	25.3	33.7	23.9	29.7	25.6	21.8
Nd	85.1	91.6	109.6	100.6	98.2	134.2	93.7	117.2	97.2	86.0
Sm	19.4	18.9	22.0	21.2	20.6	27.9	22.0	24.1	19.6	17.1
Eu	4.6	4.2	4.8	4.6	4.5	5.9	5.1	5.1	4.3	4.6
Gd	19.1	16.8	19.9	18.1	18.7	24.8	21.6	22.4	17.7	14.9
Tb	3.2	2.6	3.2	2.7	3.1	3.9	4.1	3.6	2.7	2.3
Dy	18.8	15.3	18.2	15.4	18.1	22.9	26.7	21.6	15.8	12.8
Ho	3.3	3.1	3.6	2.9	3.5	4.5	5.4	4.3	3.1	2.5
Er	8.8	8.6	9.9	8.2	10.1	12.5	14.9	12.0	8.7	7.0
Tm	1.2	1.1	1.3	1.1	1.4	1.7	2.1	1.6	1.2	1.0
Yb	7.4	7.2	8.2	7.0	8.5	10.4	13.1	10.0	7.4	6.3
Lu	1.1	1.0	1.1	1.0	1.2	1.5	1.8	1.4	1.1	1.0
Hf	18.5	17.9	22.2	18.9	20.8	27.6	35.5	27.7	18.5	14.1
Ta	5.4	5.7	6.7	5.5	6.4	7.4	9.9	8.1	5.5	5.1
Th	13.1	12.6	15.8	17.2	14.2	19.0	21.1	22.5	13.8	10.7
U	2.7	2.8	3.2	3.8	3.7	4.4	5.3	4.4	3.2	2.5
Eu/Eu*	0.73	0.70	0.69	0.71	0.68	0.67	0.71	0.66	0.69	0.87
$(La/Sm)_N$	2.8	3.0	3.1	3.0	3.0	3.0	2.2	3.1	3.3	3.2
$(La/Yb)_N$	8.3	8.8	9.4	10.1	8.0	8.8	4.1	8.2	9.7	9.6

GS03-023	GS03-024A	GS03-026	GS03-107	GS03-108	GS03-109	GS03-110	GS03-112	GS03-113	GS03-114	GS03-117
Panzhihua	Panzhihua	Panzhihua	Woshui	Woshui	Woshui	Woshui	Woshui	Woshui	Woshui	Woshui
65.63	66.65	63.78	63.06	62.02	63.73	60.80	62.18	61.47	61.54	62.10
0.62	0.71	0.83	0.82	1.06	0.72	1.16	0.94	1.05	1.10	0.94
13.64	13.41	13.72	17.15	16.59	17.36	16.35	16.81	16.59	16.82	16.88
6.51	7.60	8.80	3.33	4.57	3.06	4.97	4.00	4.60	4.81	4.22
0.21	0.26	0.31	0.14	0.19	0.13	0.22	0.17	0.19	0.20	0.18
0.18	0.19	0.57	0.72	1.00	0.63	1.15	0.91	1.06	1.10	0.94
0.81	1.49	1.56	1.41	2.04	1.30	2.23	1.71	1.99	2.03	1.78
5.87	5.62	4.91	7.46	7.13	7.55	7.13	7.29	7.18	7.38	7.47
4.83	4.12	2.46	4.04	3.75	4.07	3.70	3.90	3.76	3.75	4.03
0.02	0.03	0.12	0.15	0.21	0.13	0.25	0.20	0.22	0.24	0.20
1.35	0.75	1.89	0.39	0.42	0.29	0.64	0.63	0.67	0.36	0.13
99.67	100.83	98.93	98.66	98.99	98.96	98.59	98.74	98.80	99.33	98.87
0.83	0.82	1.01	0.89	0.85	0.90	0.83	0.87	0.85	0.85	0.85
1.09	1.02	0.78	0.97	0.95	0.97	0.96	0.96	0.96	0.96	0.99
0.82	0.73	0.50	0.54	0.53	0.54	0.52	0.53	0.52	0.51	0.54
0.97	0.97	0.93	0.81	0.80	0.81	0.80	0.80	0.80	0.80	0.80
16	14	19	11	14	13	14	13	13	12	16
2	2	2	20	30	18	35	26	30	30	26
3	4	6	3	4	4	9	3	4	4	3
0	1	1	1	2	1	2	2	2	2	2
2	1	2	3	5	3	8	6	5	3	3
8	7	8	7	9	6	11	7	8	8	8
200	230	251	97	147	106	186	120	140	185	125
37.6	36.1	36.9	30.7	31.2	30.3	31.3	31.3	31.8	31.5	26.4
96	70	46	46	40	43	37	40	39	36	34
43	59	81	593	646	603	666	617	610	634	569
68	57	70	27	35	23	38	31	34	33	29
807	635	767	300	106	142	187	110	196	108	138
74	73	76	44	48	33	51	42	46	44	40
0.6	0.3	0.1	0.2	0.1	0.2	0.2	0.1	0.1	0.1	0.1
1008	1141	535	2460	2396	2425	2505	2345	2297	2446	2101
76.4	68.3	86.7	49.1	63.2	41.6	68.6	61.0	69.0	70.4	64.1
180.7	145.9	164.3	106.5	143.0	91.4	153.8	135.5	150.9	152.8	140.0
20.6	19.0	22.7	14.1	18.6	11.9	20.5	17.5	19.4	19.7	17.9
80.2	74.7	90.2	56.6	77.3	48.7	84.8	71.2	79.8	80.3	73.7
16.5	15.8	18.3	10.5	14.3	8.9	15.6	12.8	14.5	14.3	13.2
4.2	4.8	5.7	5.0	5.8	4.7	6.0	5.3	5.7	5.6	4.7
14.7	13.7	16.3	9.6	12.9	8.3	14.1	11.8	13.1	13.2	13.1
2.4	2.1	2.5	1.3	1.8	1.1	1.9	1.5	1.7	1.7	1.6
13.8	12.1	14.4	5.9	8.0	5.1	8.7	6.9	7.8	7.7	7.7
2.7	2.3	2.8	1.1	1.4	0.9	1.6	1.3	1.4	1.4	1.3
7.7	6.6	7.9	3.0	3.8	2.4	4.2	3.3	3.7	3.5	4.1
1.0	0.9	1.1	0.4	0.5	0.3	0.5	0.4	0.5	0.4	0.4
6.6	6.0	6.8	2.2	2.6	1.8	3.0	2.3	2.6	2.4	2.7
1.0	0.9	0.9	0.3	0.4	0.2	0.4	0.3	0.4	0.4	0.4
16.2	12.8	15.9	6.3	3.1	3.4	4.4	2.8	4.5	2.6	4.0
5.2	4.6	5.2	2.4	2.6	2.1	2.5	2.3	2.4	2.1	2.6
11.9	8.8	11.6	2.3	2	1.8	2.1	2.9	2.0	1.4	2.5
3	2.2	2.9	0.7	0.6	0.5	0.5	0.5	0.5	0.4	0.6
0.80	0.97	0.98	1.51	1.27	1.63	1.22	1.29	1.23	1.23	1.07
3.0	2.8	3.1	3.0	2.8	3.0	2.8	3.1	3.1	3.2	3.1
8.3	8.2	9.1	15.9	17.3	16.9	16.7	18.9	18.9	21.1	17.4

(continued on next page)

Table 2 (*continued*)

Sample	GS03-118	GS03-119	GS03-120	GS03-121	GS05-049	GS05-048	GS05-047	GS05-046	GS05-071	GS05-066
Location	Woshui	Woshui	Woshui	Woshui	Woshui	Woshui	Woshui	Woshui	Woshui	Woshui
SiO_2 (wt.%)	62.25	62.01	62.29	62.25	62.65	62.60	62.21	61.76	62.57	62.83
TiO_2	0.92	0.99	0.94	0.89	0.92	0.88	0.96	1.01	0.82	0.75
Al_2O_3	16.88	16.86	16.94	17.00	16.99	17.16	16.72	16.63	17.95	17.81
Fe_2O_3t	4.07	4.18	4.14	3.89	3.85	3.77	4.06	4.29	3.48	3.21
MnO	0.17	0.18	0.17	0.16	0.17	0.17	0.18	0.19	0.14	0.13
MgO	0.88	1.02	0.89	0.91	0.84	0.84	0.91	0.96	0.77	0.72
CaO	1.67	1.85	1.76	1.65	1.38	1.34	1.46	1.53	1.53	1.44
Na_2O	7.43	7.37	7.08	7.49	7.34	7.30	7.26	7.37	7.44	7.34
K_2O	3.87	3.86	3.74	3.88	4.33	4.15	4.26	4.32	3.93	3.85
P_2O_5	0.19	0.22	0.20	0.19	0.20	0.20	0.20	0.22	0.20	0.18
LOI	0.42	0.41	0.63	0.52	0.42	0.43	0.52	0.29	0.28	0.25
Total	98.76	98.95	98.78	98.83	99.08	98.84	98.73	98.55	99.10	98.51
ANCK	0.87	0.86	0.90	0.87	0.88	0.91	0.87	0.85	0.93	0.94
Na+K/Al	0.97	0.97	0.93	0.97	0.99	0.96	0.99	1.01	0.92	0.91
K_2O/Na_2O	0.52	0.52	0.53	0.52	0.59	0.57	0.59	0.59	0.53	0.52
Fe*	0.81	0.79	0.81	0.79	0.80	0.80	0.80	0.80	0.80	0.80
Sc (ppm)	14	14	15	15	11	11	12	12	8	9
V	27	25	29	26	26	20	22	28	20	19
Cr	8	4	3	4	2	0	0	0	0	0
Co	2	2	2	2	3	3	3	3	1	1
Ni	5	3	3	3	27	11	10	10	19	48
Cu	8	7	8	7	5	3	3	3	5	14
Zn	212	123	161	121	120	103	112	118	62	70
Ga	31.8	31.1	31.5	31.2	26.7	22.2	26.6	25.5	19.4	23.4
Rb	47	41	43	42	99	63	57	68	29	34
Sr	607	636	623	644	451	424	407	448	502	541
Y	32	30	31	29	37	28	37	35	21	18
Zr	181	161	140	114	244	242	251	285	62	59
Nb	41	39	46	39	61	48	69	74	28	26
Cs	0.3	0.1	0.2	0.1	0.6	0.4	0.3	0.3	0.0	0.1
Ba	2338	2460	2369	2450	1795	1720	1718	1511	1284	2279
La	60.9	58.1	66.1	58.0	70.9	58.9	96.4	59.1	40.5	44.0
Ce	134.9	126.2	140.7	126.9	144.4	120.7	173.4	134.6	76.0	88.4
Pr	17.8	16.4	18.0	16.8	17.9	16.2	24.1	21.2	11.7	13.5
Nd	73.5	68.3	73.1	69.1	74.8	62.6	95.2	84.4	50.2	54.7
Sm	13.1	12.4	13.0	12.5	14.2	11.3	13.5	14.2	9.0	9.1
Eu	5.3	5.4	5.3	5.3	4.8	4.7	5.2	4.9	4.7	4.8
Gd	12.3	11.5	12.0	11.5	8.1	8.0	9.5	8.5	5.4	5.7
Tb	1.6	1.5	1.6	1.5	1.4	1.3	1.7	1.6	0.9	1.0
Dy	7.4	6.8	6.9	6.9	6.9	6.4	8.3	7.7	4.7	4.6
Ho	1.3	1.2	1.2	1.2	1.2	1.1	1.5	1.3	0.9	0.9
Er	3.4	3.2	3.3	3.1	3.5	2.9	4.0	3.9	2.1	2.0
Tm	0.4	0.4	0.4	0.4	0.5	0.4	0.5	0.5	0.3	0.2
Yb	2.4	2.3	2.4	2.1	2.8	2.6	2.7	3.1	1.5	1.4
Lu	0.4	0.3	0.4	0.3	0.4	0.3	0.4	0.4	0.2	0.2
Hf	4.3	3.8	3.5	2.9	5.4	4.7	6.8	6.2	1.5	1.5
Ta	1.6	2.1	2.2	2.1	4.0	3.3	5.1	4.3	1.9	1.7
Th	2.1	1.7	2.2	1.9	5.5	3.5	6.4	4.7	1.2	1.1
U	0.6	0.4	0.5	0.4	1.3	1.0	1.5	1.3	0.2	0.3
Eu/Eu*	1.25	1.36	1.28	1.33	1.24	1.43	1.33	1.27	1.91	1.90
$(La/Sm)_N$	3.0	3.0	3.3	3.0	3.2	3.4	4.6	2.7	2.9	3.1
$(La/Yb)_N$	18.4	18.3	19.9	19.6	18.3	16.2	25.3	13.6	19.6	22.0

GS05-063	GS05-068	GS05-067	GS05-074	GS05-072	GS05-073	GS05-065	GS05-064	GS05-070	GS05-069
Woshui	Woshui	Woshui	Woshui	Woshui	Woshui	Woshui	Woshui	Woshui	Woshui
61.79	61.11	61.49	61.67	62.15	61.89	62.03	61.06	61.88	65.28
0.92	1.13	1.06	1.01	0.89	1.02	0.90	0.98	0.94	0.27
17.51	16.96	17.16	17.34	17.64	17.27	17.49	17.37	17.44	18.62
4.21	4.99	4.54	4.27	3.80	4.46	3.94	4.44	4.08	1.11
0.17	0.20	0.19	0.18	0.16	0.19	0.16	0.18	0.16	0.03
0.91	1.13	1.05	0.97	0.82	1.00	0.87	1.00	0.84	0.23
1.92	2.13	1.97	1.82	1.69	1.93	1.70	1.89	1.73	0.45
7.24	7.00	7.18	7.20	7.24	7.13	7.24	7.19	7.26	7.77
3.76	3.61	3.71	3.66	3.78	3.71	3.76	3.79	3.82	4.56
0.26	0.32	0.29	0.28	0.22	0.28	0.23	0.27	0.25	0.00
0.34	0.27	0.22	0.35	0.15	0.16	0.39	0.54	0.28	0.36
99.04	98.85	98.86	98.77	98.53	99.04	98.72	98.72	98.68	98.69
0.90	0.88	0.88	0.91	0.92	0.90	0.92	0.90	0.91	1.00
0.91	0.91	0.92	0.91	0.91	0.91	0.91	0.92	0.92	0.95
0.52	0.52	0.52	0.51	0.52	0.52	0.52	0.53	0.53	0.59
0.81	0.80	0.80	0.80	0.81	0.80	0.80	0.80	0.81	0.81
13	10	10	9	8	12	11	12	8	12
26	38	29	24	23	31	25	30	24	3
2	0	0	0	0	2	2	4	0	0
1	2	1	1	1	2	1	1	1	1
42	37	32	31	28	35	85	83	57	60
13	12	10	10	8	11	29	24	18	16
103	128	105	85	75	130	95	108	100	13
26.2	25.4	25.0	22.4	22.3	28.1	24.4	24.6	22.5	37.2
34	30	33	25	29	33	35	34	31	48
682	650	609	451	563	627	636	595	602	270
28	33	34	27	24	31	29	30	29	16
123	103	73	36	78	80	94	81	80	20
33	42	38	27	34	32	35	37	30	17
0.1	0.1	0.1	0.1	0.0	0.1	0.1	0.1	0.1	0.0
1544	1959	1658	1462	1666	2168	2187	2310	1998	1023
58.8	68.0	57.7	47.6	50.9	62.2	51.9	54.8	52.0	45.9
105.3	137.5	114.6	107.5	97.6	110.0	124.9	124.4	103.5	90.0
17.5	20.4	20.9	16.5	14.9	21.7	17.3	18.9	15.4	15.0
75.9	80.8	82.5	58.6	59.9	89.8	71.7	71.4	76.5	71.6
14.3	13.7	15.1	10.4	10.5	14.9	12.6	13.1	12.4	11.8
6.5	6.4	7.0	4.9	5.3	7.1	6.5	5.2	5.2	2.5
8.4	9.4	8.4	7.0	7.0	9.1	7.5	8.1	8.3	6.0
1.4	1.6	1.5	1.2	1.2	1.6	1.4	1.5	1.4	1.1
7.2	7.9	7.6	5.8	6.1	8.0	7.9	6.9	6.3	5.2
1.2	1.4	1.2	1.0	1.1	1.4	1.3	1.2	1.1	0.8
3.0	3.5	2.8	2.6	2.4	3.3	3.3	3.2	2.8	1.7
0.4	0.4	0.3	0.3	0.3	0.4	0.4	0.4	0.4	0.2
2.2	2.4	2.2	1.6	1.7	2.1	2.4	2.0	2.1	1.0
0.4	0.4	0.3	0.3	0.3	0.3	0.3	0.3	0.3	0.1
2.8	2.4	1.7	0.9	2.3	2.0	2.4	1.7	2.0	1.1
2.0	2.4	2.3	1.5	2.1	2.1	2.4	2.1	1.8	1.9
1.4	1.3	1.1	0.6	1.8	1.3	1.3	1.0	1.1	5.0
0.3	0.4	0.3	0.2	0.6	0.3	0.4	0.3	0.4	0.8
1.67	1.62	1.73	1.64	1.79	1.72	1.88	1.43	1.47	0.82
2.7	3.2	2.5	2.9	3.1	2.7	2.7	2.7	2.7	2.5
19.4	20.5	19.0	20.8	21.1	21.0	15.8	19.7	18.0	32.0

Table 3
Comparison of certified reference standards and results

Sample	AMH-1		GBPG-1		OU-6		AGV-2		G-2	
Notes	Certified	This work	Certified	This Work	Certified	This Work	Certified	This work	Certified	This work
Li (ppm)	11.86	12.2	20.97	21.97	95.3	100.5	11	11.1	34	36.4
Be	1.19	1.22	0.90	0.78	2.53	2.44	2.3	2.3	2.5	2.6
Sc	13.48`	13.2	13.93	15.50	23.1	22.2	13	14.3	3.5	11.4
Cr	40.89	41.58	181.4	180.0	70.7	78.0	17	17.9	8.7	8.6
Co	18.68	18.7	19.5	19.78	29.2	29.1	16	15.1	4.6	4.7
Ni	32.36	33.6	59.6	58.24	40.2	41.4	19	22.0	5	6.5
Cu	30.2	30.4	30.0	30.4	40.4	42.74	53	49.5	11	13.4
Zn	66.9	73.0	80.3	85.5	111.4	103.1	86	94.2	86	83.1
Ga	20.49	20.3	18.6	20.0	24.17	26.01	20	20.2	23	21.1
Rb	18.31	18.8	56.2	58.0	121.3	125.5	68.6	70.3	170	165.2
Sr	545.4	547.7	363.5	367.8	131.7	135.5	658	699.2	478	477.4
Y	16.44	15.1	18.0	17.6	27.75	26.94	20	21.4	11	10.1
Zr	146	144.9	231.8	226.1	174.2	177.2	230	235.1	309	330.8
Nb	8.32	8.0	9.93	9.77	14.49	14.33	15	14.5	12	13.0
Cs	0.24	0.24	0.32	0.33	8.10	8.27	1.16	1.2	1.34	1.41
Ba	322.3	317.3	908.0	918.96	480	478.32	1140	1135	1880	1839
La	15.87	16.3	52.95	51.0	33.2	34.28	38	38.9	89	84.8
Ce	33.03	33.4	103.20	98.0	77.1	78.43	68	73.7	160	170.0
Pr	4.21	4.3	11.45	11.52	7.91	8.29	8.3	8.6	18	18.3
Nd	17.69	17.3	43.30	41.2	30.2	30.8	30	31.2	55	55.4
Sm	3.68	3.7	6.79	6.5	6.01	6.18	5.7	5.7	7.2	7.5
Eu	1.16	1.17	1.79	1.74	1.36	1.38	1.54	1.55	1.4	1.5
Gd	3.34	3.25	4.74	4.97	5.30	5.38	4.69	4.90	4.3	4.2
Tb	0.51	0.51	0.60	0.60	0.86	0.86	0.64	0.67	0.48	0.50
Dy	2.84	2.76	3.26	3.07	5.06	5.04	3.6	3.6	2.4	2.4
Ho	0.57	0.56	0.69	0.65	1.04	1.02	0.71	0.76	0.4	0.4
Er	1.52	1.52	2.01	2.05	2.93	3.04	1.79	1.78	0.92	0.96
Tm	0.21	0.21	0.30	0.31	0.45	0.46	0.26	0.27	0.18[a]	0.13
Yb	1.37	1.43	2.03	2.12	2.98	3.10	1.6	1.7	0.8	0.8
Lu	0.21	0.21	0.31	0.32	0.45	0.48	0.25	0.26	0.11	0.12
Hf	3.7	3.7	6.07	5.58	4.70	4.89	5.08	5.51	7.9	8.7
Ta	0.64	0.58	0.40	0.41	1.02	1.07	0.89	1.02	0.5	0.93
Pb	9.85	8.7	14.10	14.73	28.80	29.73	13	13.3	30	30.4
Th	2.64	2.51	11.23	11.33	11.3	11.6	6.1	6.2	25	25.4
U	0.89	0.90	0.90	0.88	1.92	2.04	1.88	1.99	2.07	2.04

[a]Provisional value.

3.4. Ailanghe granitic intrusion

The rocks in this intrusion consist mostly of feldspar and quartz with minor hornblende. The feldspars include 35–40% alkali feldspar and 20–25% plagioclase feldspar. The alkali feldspar is anhedral to subhedral with blocky or tabular shapes ~0.5 to 1.5 cm long. Both perthite exsolution and microcline twinning are present however perthitic feldspar is significantly more abundant. The plagioclase feldspar is subhedral to euhedral and has rectangular shapes ~0.3–0.7 cm long. The plagioclase typically shows saussurite alteration and in a few cases is bent. Quartz comprises ~35% of the mineral mode and is usually anhedral and rounded. The grain size varies from <0.1 cm to 0.8 cm. Occasionally smaller grains of quartz occur along the grain boundaries of the feldspars or as inclusions within the feldspars. The hornblende and biotite are the primary mafic minerals and represent a combined 5% of the mineral mode. The hornblende is interstitial to quartz and feldspar and is <0.5 cm in length. Typically hornblende is elongate however it may be blocky or rounded in shape and altered to chlorite. Biotite is typically forms euhedral tabular crystals and varies in modal abundance. There are accessory (≪1%) amounts of apatite, oxides and zircon and rare occurrences of muscovite and titanite.

4. Analytical methods

4.1. SHRIMP zircon analyses

Conventional heavy liquid and magnetic techniques were used to separate zircons. The zircons were mounted in epoxy, polished, coated with gold and photographed in transmitted and reflected light to identify individual grains. U–Pb isotopic ratios of zircon separates were measured using the SHRIMP II at the Chinese Academy of Geological Sciences, Beijing, China (Liu et al., 2006; Wan et al., 2006) (Table 1). The measured isotopic ratios were reduced off-line using standard techniques (see Claoue-Long et al., 1995) and the U–Pb ages were normalized to a value of 417 Ma determined by conventional U–Pb analysis of zircon standard TEMORA 1 (Black et al., 2003a,b). Common Pb was corrected using the methods of Compston et al. (1984). The $^{206}Pb/^{238}U$ and $^{207}Pb/^{235}U$ data were corrected for uncertainties associated with the measurements of the TEMORA 1 standard.

4.2. Whole rock geochemical analyses

Major element analyses were carried out using X-ray fluorescence at The University of Hong Kong on fused glass discs (Table 2). Trace elements were analyzed by a VG Elemenal PlasmaQuad Excell inductively coupled plasma mass spectrometer (ICP-MS) with the dilution of 1:2000 also at The University of Hong Kong. Samples were digested using a mixed HF acid and HNO_3 in a high-pressure bomb and ^{103}Rh was used as an internal standard to correct the fluctuations and matrix effects (Qi et al., 2000). The $^{137}Ba^{16}O/^{137}Ba$ ratio of this instrument is about 0.0006 with a semi-conducting cooler and interference of $^{136}Ba^{16}O^{1}H$ to ^{153}Eu is negligible. The BaO interferences were monitored by a Ba solution and verify the Eu values with the ratio of BaO/Ba every time the concentration of Eu was analyzed. International standards were analyzed concurrently to check the results of the verified value of Eu. The differences between the certified Eu values of these standards and Eu values determined in our lab are no more than 5%.

The precisions for the major element results are better than 5% and 10% for trace elements. Standard reference materials for the major elements were BHVO-2 (basalt), JGB-2 (gabbro) and GSR-1 (granite). For the trace element analysis, the standard reference materials AMH-1 (Mount Hood andesite), GBPG-1 (garnet-biotite plagiogneiss), AGV-2 (andesite), G-2 (granite) and OU-6 (Prerhyn slate) (Thompson et al., 1999; Potts et al., 2000, 2001; USGS Geochemical Reference Standards) were analyzed (Table 3). The precisions for most trace elements are better than 10%.

4.3. Sm–Nd and Rb–Sr isotope analyses

Whole rock radiogenic Sr and Nd isotopes were determined for five samples each from the Panzhihua, the Taihe, the Woshui plutons and three from the Ailanghe pluton. The $\varepsilon Nd_{(T)}$ and $_{I}Sr$ values have been corrected to their SHRIMP U/Pb age date respectively unless otherwise stated (Table 4).

Approximately 100–150 mg of whole rock powder was dissolved in a mixture of HF-$HClO_4$ for Sr–Nd isotopic analysis following the procedure of Zhang et al. (2001). Separation of the required elements for isotopic analysis was by cation exchange. Rb, Sr, Sm, and Nd concentrations were obtained by isotope dilution; a mixed ^{87}Rb–^{84}Sr–^{149}Sm–^{150}Nd spike solution was used. Strontium and REEs were separated on quartz columns with a 5 ml resin bed of AG 50 W-X12, 200-400 mesh. Neodymium was separated from other REEs on quartz columns using 1.7 ml teflon powder+reagent as a cation exchange medium. Procedural blanks were <200 pg for Sr and <50 pg for Nd. For the measurements of isotopic composition, Sr was loaded with a Ta-Hf activator on a single W filament and Nd was loaded as phosphates and measured in a Re-double-filament configuration. $^{143}Nd/^{144}Nd$ ratios were normalized to $^{146}Nd/^{144}Nd=0.7219$ and $^{87}Sr/^{86}Sr$ ratios to $^{86}Sr/^{88}Sr=0.1194$. Isotopic ratios were measured using a Finnigan MAT-262 thermal ionization mass spectrometer (TIMS) in the Laboratory for Radiogenic Isotope Geochemistry, Institute of Geology and Geophysics, Chinese Academy of Sciences, Beijing. Raw data obtained were calculated using the Isoplot program (Ludwig, 2001), giving 2σ error. The 2σ values for all samples are between 11 and 14. Detailed procedure of chemical separation and measurement are described in Chen et al. (2000, 2002).

5. Results

5.1. SHRIMP zircon U–Pb age dating results

Previously published SHRIMP zircon ages of some plutons are 261±2 Ma for Taihe (Luo et al., 2006); 251±6 for Ailanghe (Zhong et al., 2007); ~260 Ma for the Baima syenite and 252±2 Ma for the Huangcao syenite (Shellnutt and Zhou, 2006a,b).

One sample GS05-065, a syenite from Woshui, was used for determining the age using SHRIMP zircon U–Pb

Table 4
Nd and Sr radiogenic isotope compositions for the Permian Panxi granites

Sample	Rb (ppm)	Sr (ppm)	$(^{87}Rb/^{86}Sr)_m$	$(^{87}Sr/^{86}Sr)_m$	$(^{87}Sr/^{86}Sr)_i$	Sm (ppm)	Nd (ppm)	$(^{147}Sm/^{144}Nd)_m$	$(^{143}Nd/^{144}Nd)_m$	εNd
GS04-057	143.4	15.98	26.08	0.785499	0.688637	24.48	129.4	0.1145	0.512594	+1.9
GS04-059	144	13.64	30.70	0.802919	0.688928	18.43	94.53	0.1180	0.512596	+1.8
GS04-066	140.6	13.35	30.65	0.805694	0.691888	17.99	88.88	0.1225	0.512607	+1.9
GS04-155	137.7	18.51	21.72	0.778467	0.697810	20.03	104.3	0.1163	0.512597	+1.9
GS04-148	125.4	8.922	41.13	0.837563	0.684844	19.91	97.32	0.1238	0.512592	+1.5
GS03-009	79.15	24.43	9.3943	0.731032	0.696284	19.70	95.83	0.1243	0.512662	+2.9
GS03-010	96.32	40.99	6.7578	0.726337	0.701340	21.22	105.4	0.1217	0.512625	+2.2
GS03-013	89.28	38.95	6.6319	0.728226	0.703695	19.62	87.62	0.1353	0.512653	+2.3
GS03-014	101.1	32.48	9.0274	0.734007	0.700616	19.57	94.31	0.1255	0.512652	+2.6
GS03-015	98.57	34.25	8.3495	0.734137	0.703254	22.67	110.7	0.1238	0.512661	+2.9
GS03-108	39.69	663	0.1732	0.705054	0.704413	13.49	72.08	0.1132	0.512638	+2.7
GS03-110	36.67	683.8	0.1551	0.704988	0.704414	15.14	80.81	0.1132	0.512636	+2.6
GS03-114	41.37	661.3	0.1809	0.704988	0.704319	14.24	78.88	0.1092	0.512630	+2.7
GS03-117	46.14	629	0.2122	0.705222	0.704437	13.06	70.58	0.1118	0.512759	+3.1
GS03-119	42.86	648.1	0.1913	0.705104	0.704396	12.81	71.56	0.1083	0.512633	+2.7
GS04-091*	263.5	51.49	14.87	0.753722	0.700628	3.635	16.23	0.1354	0.512192	−6.7
GS04-095*	228.9	54.42	12.21	0.746818	0.703222	8.027	46.05	0.1054	0.512172	−6.2
GS04-097*	212.2	117.2	5.249	0.729895	0.711007	5.204	30.26	0.1040	0.512194	−5.7

$(87Rb/86Sr)_m$, $(87Sr/86Sr)_m$, $(147Sm/144Nd)_m$ and $(143Nd/144Nd)_m$-measured isotopic ratios, respectively. $(87Sr/86Sr)i$ and εNd are age calculated to 252* and 260 Ma respectively. Concentrations of Nd, Sm, Rb and Sr were determined by thermal ion mass spectrometer. All isotope values have 2σ of 16 or less.

age dating techniques. The zircon crystals tend to have angular shapes. Their Th/U ratios vary from 0.15 to 1.96 with an average of 0.88 and standard deviation of 0.39. A concordia plot (Fig. 5) yields a mean $^{206}Pb/^{238}U$ age of 260±2 Ma (0.87% 2σ) with a MSWD of 0.66.

5.2. Whole rock geochemistry

Since the term A-type granite was introduced by Loiselle and Wones (1979) it has been a subject of controversy and numerous studies (Collins et al., 1982; Clemens et al., 1986; Whalen et al., 1987; Sylvester, 1989; Creaser et al., 1991; Hogan et al., 1992; Nyman et al., 1994; Poitrasson et al., 1995; King et al., 1997; Frost et al., 2001). The term originally was used to distinguish within-plate or anorogenic granites from other types of granites. The anorogenic granitoids have high Fe* (FeO/FeO+MgO), K_2O/Na_2O, enriched REE (except Eu) and have low concentrations of Co, Sc, Cr, Ni, Ba, Sr, Eu and low fO_2. Even though there are known discrepancies with this method of classification it still remains popular in literature and is, in general, a useful means to distinguish granites which formed from

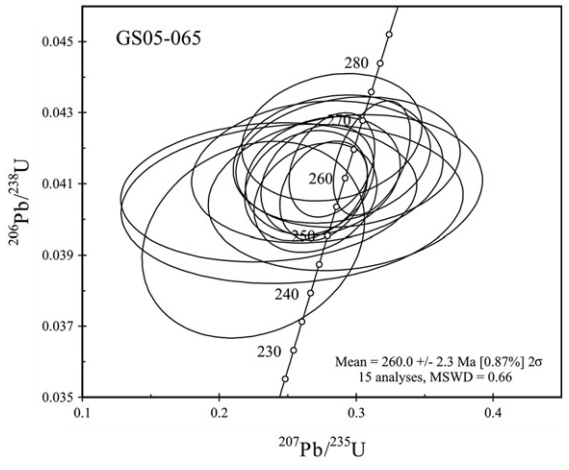

Fig. 5. Concordia plot of all SHRIMP zircon U–Pb data for sample GS05-065, a syenite from Wohsui.

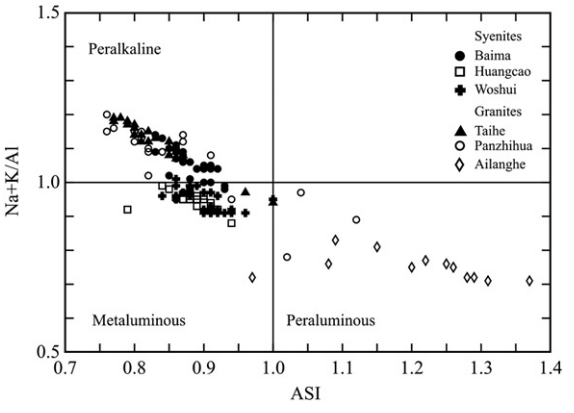

Fig. 6. Molecular Na+K/Al versus the alumina saturation index of Frost et al. (2001) for all the granitic rocks.

different igneous processes and tectonic settings (Pearce et al., 1984; Batchelor and Bowden, 1985; Hogan et al., 1992; Pearce, 1996; King et al., 1997).

Overall, the major elements of the Permian granites in Panxi show characteristic of A-type granites (Figs. 6 and 7). The Panzhihua and Taihe granites are chemically peralkaline (ASI=0.76–1.12. Na+K/Al=0.78–1.2) and have high Fe* values ranging from 0.92 to 0.99, similar to the ferroan alkalic peralkaline granitoids of Frost et al. (2001). The Woshui syenite is chemically metaluminous (ASI=0.84–1.0, Na+K/Al=0.91–1.01), has moderately high Fe* values (0.79–0.81) and is chemically similar to the ferroan alkalic metaluminous granitoids of Frost et al. (2001). The Ailanghe granite is chemically peraluminous (ASI=0.97–1.29), has high Fe* values (0.82–0.91), and is related to the ferroan calc-alkalic peraluminous granites of Frost et al. (2001) (Table 2).

5.2.1. Peralkaline plutons

Even though these plutons are 10 s of km apart, the peralkaline plutons (Panzhihua, Taihe and Baima) are all contemporaneously and spatially associated with layer mafic intrusions which host magmatic Fe-Ti-V oxide deposits. The mineralogy of the Panzhihua and Taihe granites is nearly identical to the Baima syenite. However the Baima syenites contain more aegirine and have a

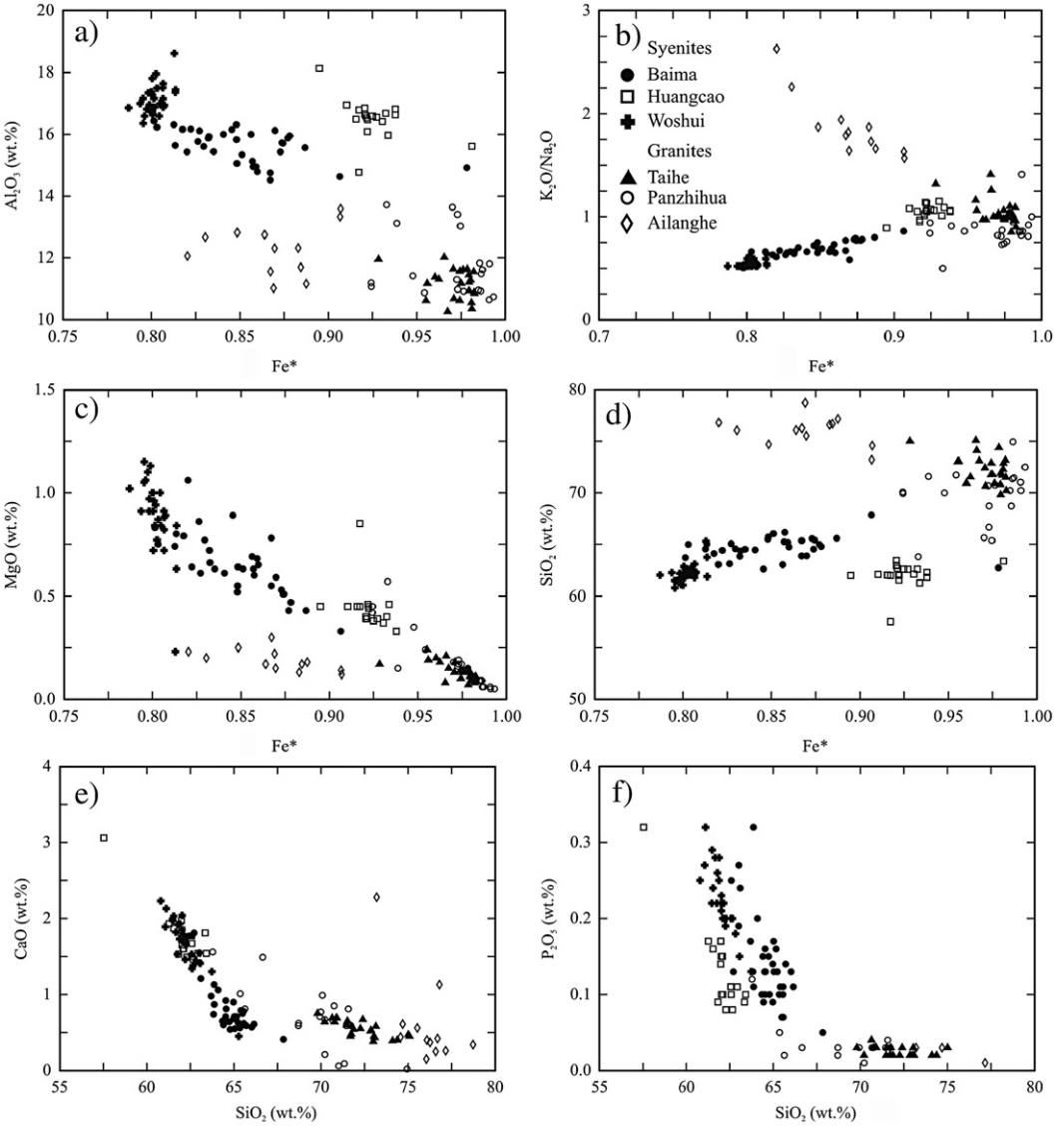

Fig. 7. Major element variations of the granites against Fe* (Fe*=FeOt/(FeOt+MgO) and SiO_2 (wt.%).

significant amount of titanite. As a consequence, the Baima syenite has lower SiO_2 wt.% and higher MnO, MgO and Na_2O wt.% than the Panzhihua and Taihe granites (Figs. 7 and 8). However, these three mutually exclusive plutons all share similar trace element compositions (Figs. 7–11) and belong to the peralkaline A-type granites (Baima syenite data unpublished).

5.2.1.1. Panzhihua granitic intrusion. Rocks from this intrusion have normative quartz, diopside, hypersthene, acmite and sodium metasilicate. Four samples (GS03-019; -020; -024 and -026) are quartz, hypersthene and corundum normative. The major elements show limited variation with respect to Fe* however there are weakly negative trends of Ti, Al, Fe, Mn, Ca and Na with respect to Si. There are no trends of Mg, P or K against Si. There are four samples from the eastern part of the intrusion (GS03-022-024; -026) which are classified as syenite on the alkalis vs. SiO_2 (wt.%) plot of LeMaitre et al. (1989) and have lower SiO_2 and higher Al_2O_3, TiO_2 and CaO. However they contain similar Na/K and Mg/Mn ratios and have similar normative mineralogy as the other samples. It is likely that the compositional variation is due to the increase of amphibole.

The Panzhihua granites contain small amounts of Sc (8–22 ppm), Cr (1–5 ppm), Co (0.2–2 ppm) and Ni

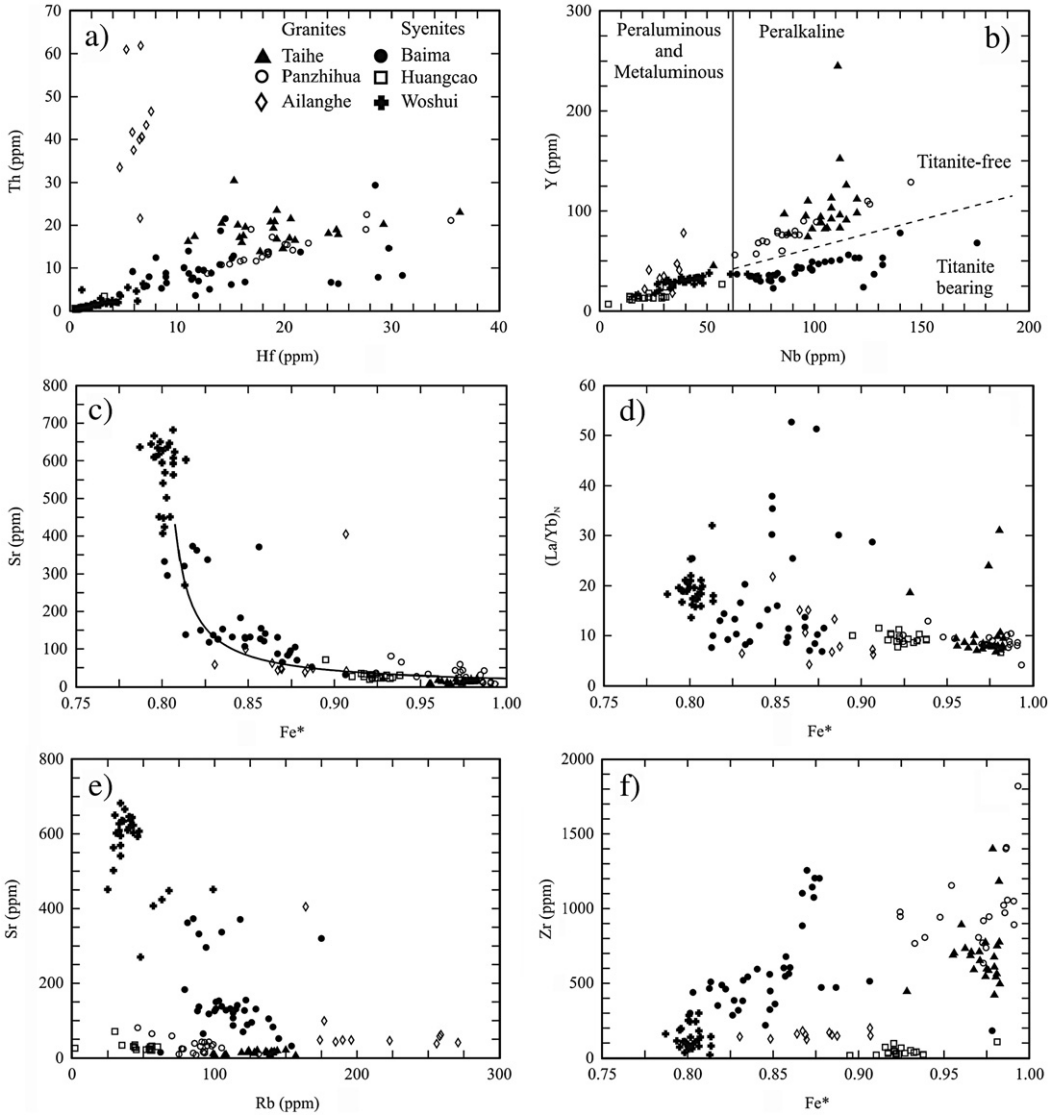

Fig. 8. Trace element variation from the Panxi granites.

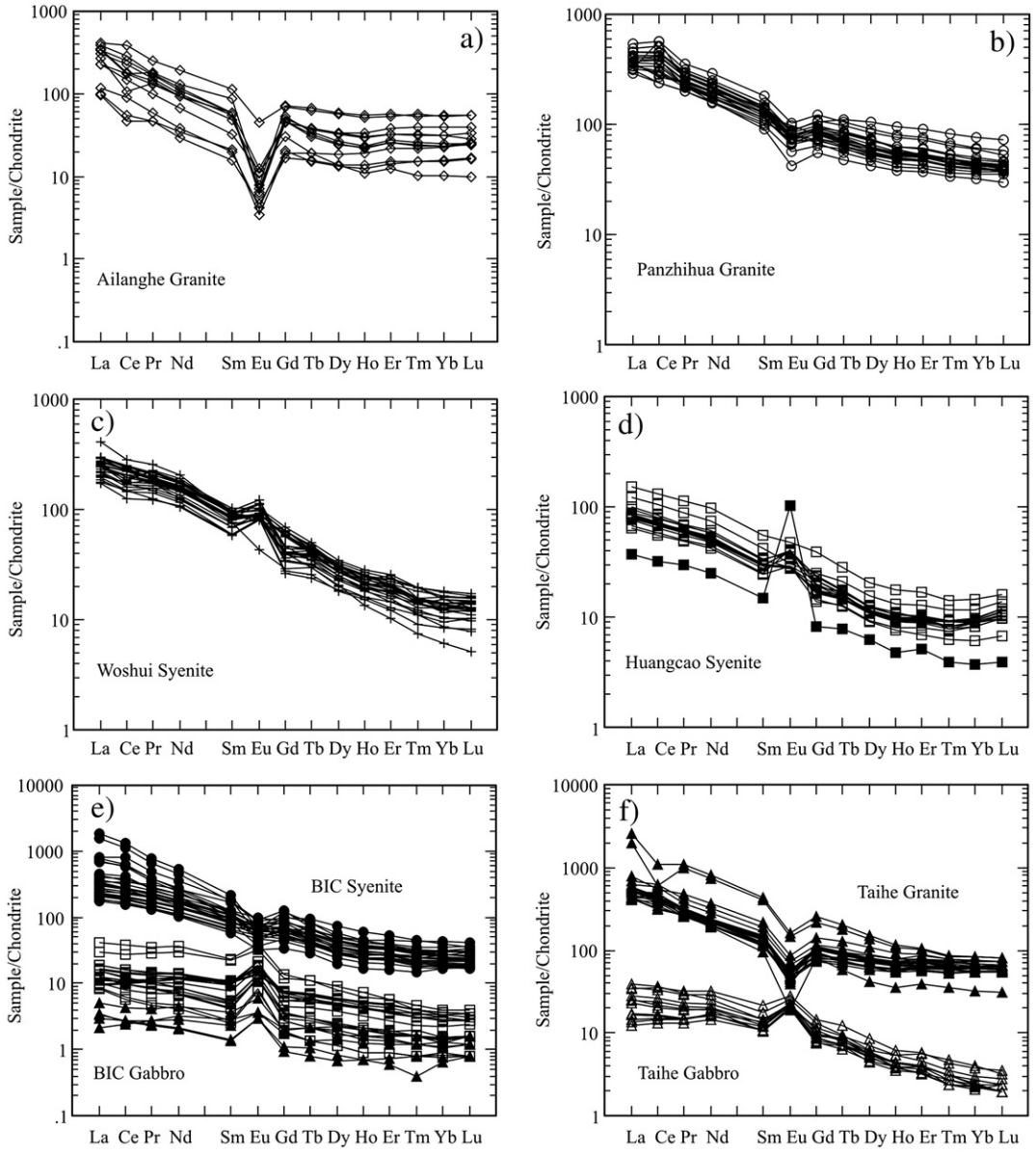

Fig. 9. Chondrite-normalized rare earth element patterns the Permian Panxi granites. Chondrite values are from Sun and McDonough (1989).

(0.6–43 ppm) similar to A-type granites. They have REE patterns enriched in LREE with a distinct negative Eu anomaly (Eu/Eu* = 0.58–0.98). $(La/Sm)_N$ and $(La/Yb)_N$ ratios range from 2.2 to 4.6 and from 4.1 to 12.9, respectively (Fig. 9). The Panzhihua granite shows a primitive mantle normalized multi-element pattern with positive anomalies of Rb, flat Th, U, Ta, Nb, REE, Hf, Zr and negative anomalies of Cs, Ba, Sr and Ti (Fig. 10). The Rb/Sr ratios are quite variable (0.6–11.5).

The Panzhihua granites have $\varepsilon Nd_{(T)}$ values ranging from +2.2 to +2.9 with $(^{143}Nd/^{144}Nd)_i$ values between 0.512418 and 0.512450. The $_{I}Sr$ values are unrealistically low, a common problem for peralkaline rocks (0.6963–0.7037) (Smith and Johnson, 1981; Long et al., 1986).

5.2.1.2. Taihe granitic intrusion. All major oxides overlap with the Panzhihua granites and show the same major element trends with respect to Fe* and Si (Fig. 7). These rocks have narrower ranges of the major elements; SiO_2 (70.3–75.77 wt.%), TiO_2 (0.23–0.66 wt.%), Al_2O_3 (9.7–12.0 wt.%), Fe_2O_3t (2.5–7.0 wt.%), MnO (≤0.20 wt.%), MgO (≤0.24 wt.%), CaO (0.39–0.75 wt.%) and total alkalis (8.0–10.2 wt.%)

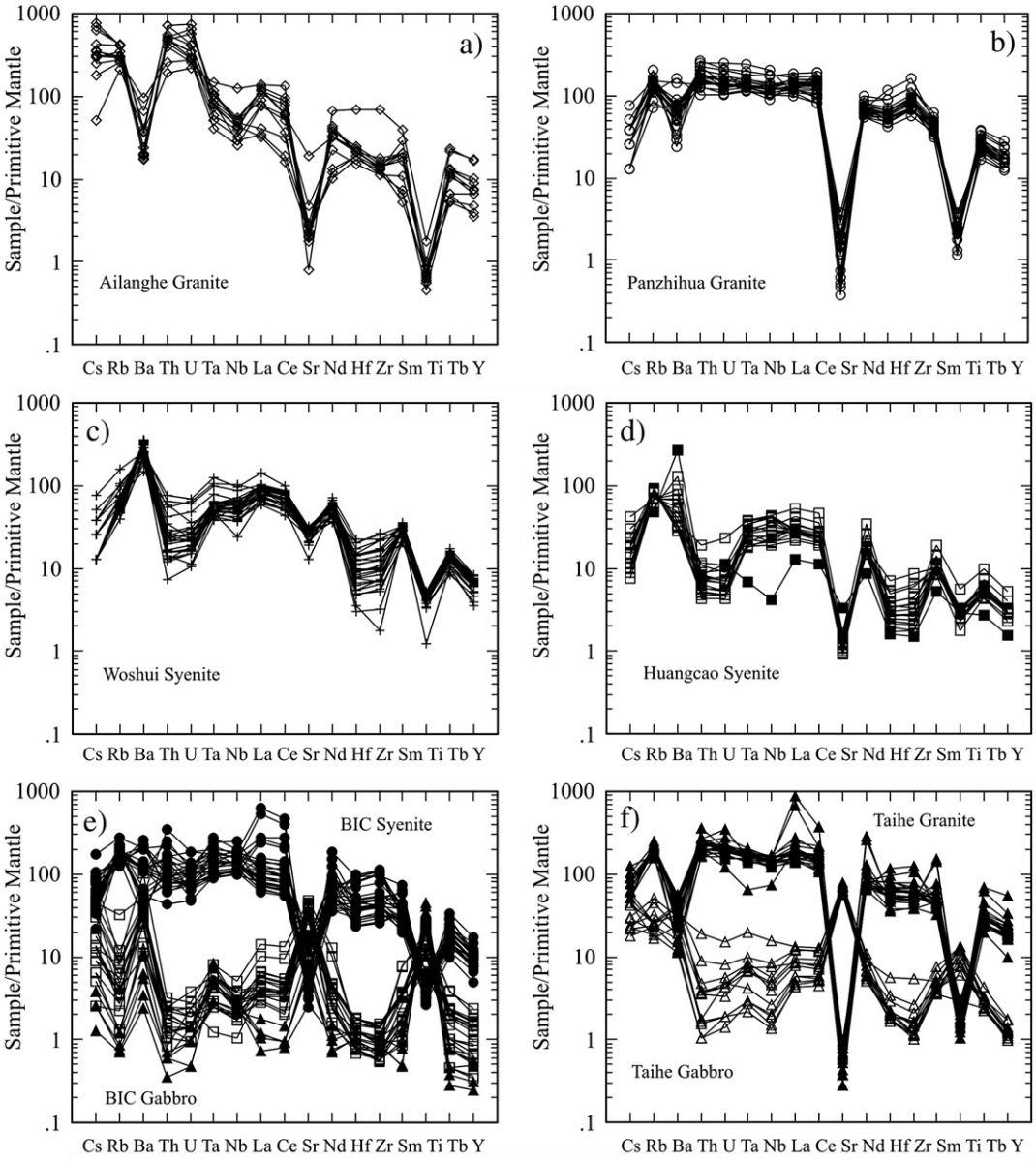

Fig. 10. Primitive mantle normalized incompatible trace element diagrams of the Permian Panxi granites. Normalizing values are from Sun and McDonough (1989).

(Fig. 7). Nearly every sample (except GS04-147) is quartz, diopside, hypersthene, acmite and Na-metasilicate normative.

The Taihe granites have trace element abundances also similar to the Panzhihua granites. The granites have low Sc (7–18 ppm), Cr (0.5–7 ppm), Co, (0.3–0.8 ppm) and Ni (1.0–38 ppm). The REE patterns are also LREE-enriched with $(La/Sm)_N$ (3.1–5.9) and $(La/Yb)_N$ (6.7–31) higher than the Panzhihua granites and have negative Eu-anomalies (Eu/Eu* = 0.22–0.50) (Fig. 9). The primitive mantle normalized incompatible trace element profile is nearly identical to the Panzhihua granite with a positive anomaly of Rb and flat Th, U, Nb, Ta, REE, Hf and Zr, and negative anomalies of Ba, Sr and Ti (Fig. 10). Their Rb/Sr ratios show significant variation and have the highest values of all the plutons (6.6–28.1).

The Taihe granites have $\varepsilon Nd_{(T)}$ values ranging from +1.5 to +1.8 with all 2σ values below 14. Their measured $^{87}Sr/^{86}Sr$ ratios are considerably high and

have a wide range (0.7785 to 0.8376). The $_{I}Sr$ calculated at 260 Ma are too low (0.6848–0.6978), very similar to the Panzhihua granite.

5.2.2. Metaluminous granites

The Woshui syenites are somewhat different from the other plutonic rocks. The rocks have a varied normative mineralogy with all samples having normative diopside. Four samples (GS03-107, -108, -109 and -120) are quartz normative with hypersthene while four other samples are nepheline and olivine normative. The remaining four samples are olivine and hypersthene normative. Some major elements, such as Ti, Fe, Mn, Mg, Ca and P, show a negative relationship with Si, whereas Al and Na show positive correlations, likely indicating a fractionation trend.

Although having Sc (11–16 ppm), Cr (3–9 ppm), Co (1–2 ppm) and Ni (2–8 ppm) generally similar to the other plutons and A-type granites, the Woshui syenites have a very different REE and trace element profiles. They have REE patterns enriched in LREE with $(La/Yb)_N$ values between 15.9 and 21.1 (Fig. 9).

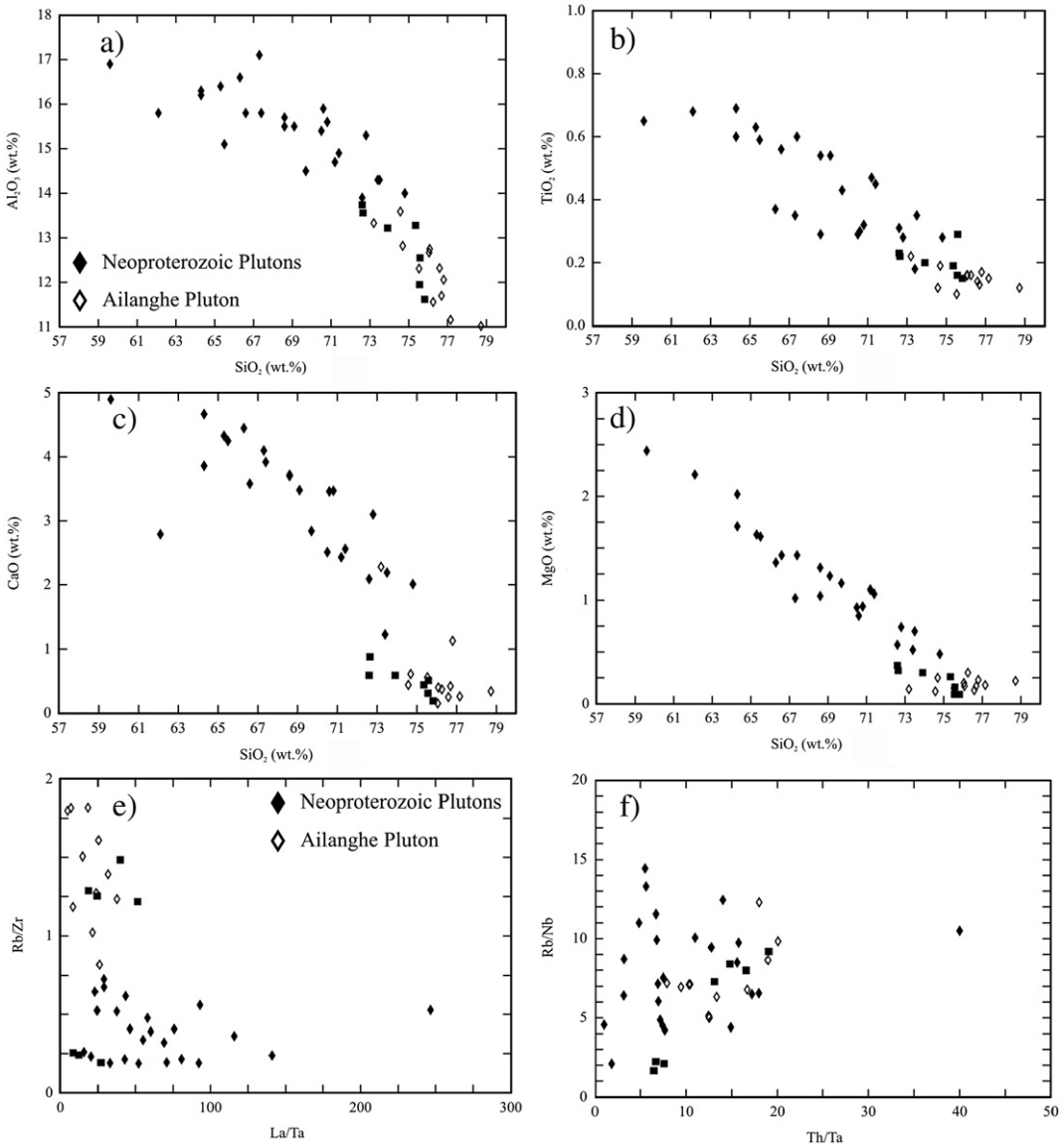

Fig. 11. Comparison of the major and trace elements of the Ailanghe granite and the Neoproterozoic granite (Ailanghe data of Zhong et al. (2007) represented by squares).

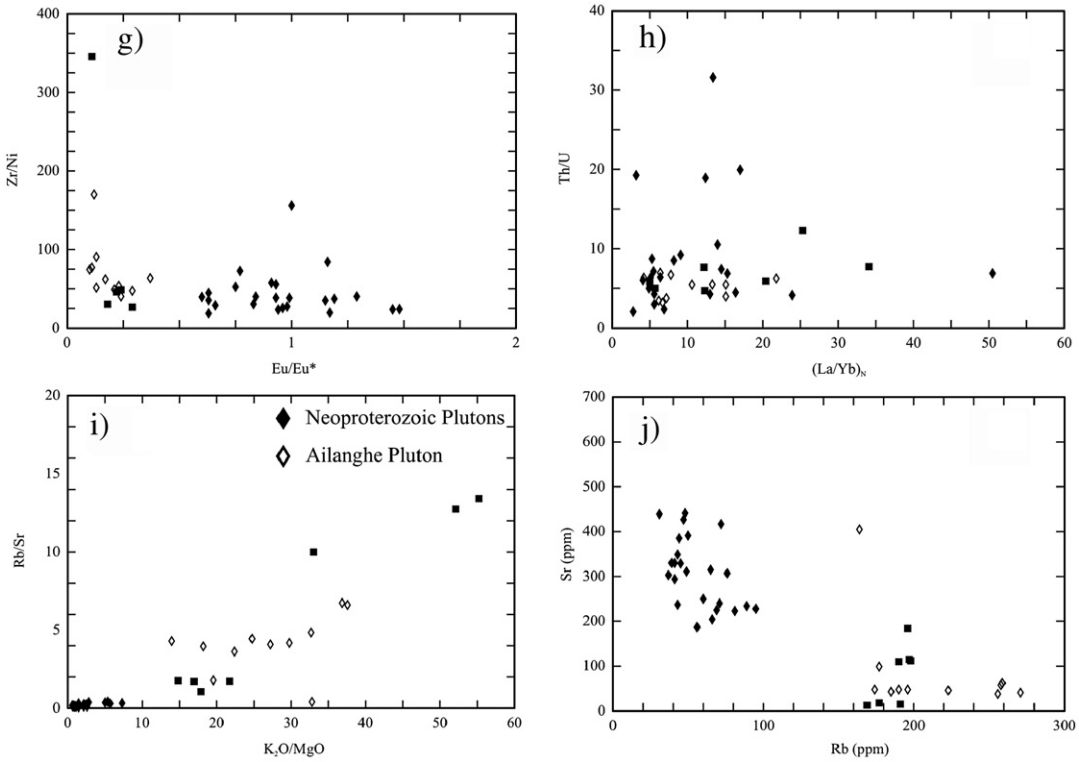

Fig. 11 (*continued*).

The $(La/Sm)_N$ (2.8–3.3) values, although similar to the other plutons, are relatively restricted. The Woshui syenite have positive Eu-anomalies (Eu/Eu*=0.82–1.91) (Fig. 9). The positive anomalies of Ba and negative anomalies of Th, U, Sr, Hf, Zr and Ti are similar to the Huangcao syenites which intruded the western portion of the Baima igneous complex (Shellnutt and Zhou, 2006b). The trace element pattern has higher normalized values of all the elements, especially Ba than the other plutons (Fig. 10). The Rb/Sr ratios are the lowest of all the plutons (<0.2).

The Woshui syenites have $\varepsilon Nd_{(T)}$ values ranging from +2.6 to +3.1 with $(^{143}Nd/^{144}Nd)_i$ values between 0.512449 and 0.512475). Unlike the peralkaline rocks, the $_{I}Sr$ values are uniform (0.7043 and 0.7044) and similar to the mafic rocks in the region.

5.2.3. Peraluminous granites

The Ailanghe granites have normative quartz, corundum and hypersthene and contains high SiO_2 ranging from 73.2–78.7 wt.% with moderate Al_2O_3 (11.0–13.6 wt.%). The L.O.I. values are all under 1.5 suggesting that there was limited mobility of major and trace elements. Although the granites have high Fe*, their Fe_2O_3t (1.1–2.2 wt.%) and MgO (0.12–0.30 wt.%) are quite low. TiO_2 is <0.22 wt.% and MnO and P_2O_5 are both ≤0.03 wt.%. Interestingly their K_2O/Na_2O ratios are quite high (1.57 to 2.26) and suggest, along with the tectonic setting, that the Ailanghe granites may represent an occurrence of peraluminous A-type granite. There is a slight positive correlation of Na with Fe* and negative correlations with Al and Na with respect to Si.

There are narrow ranges for many trace elements including Sc (10–15 ppm), V (3–13 ppm), Cr (1–5 ppm), Zn (9–38) and Ga (12–17 ppm) and moderate amounts of Y (16–78 ppm), Nb (18–39 ppm) and Th (21–61 ppm). Rb (174–271 ppm), Zr (124–201) and Ba (120–673 ppm). Sr (38–99 ppm) shows relatively moderate values with one anomalously high concentration (405 ppm) and Rb/Sr ratios of 0.4–6.8. The REE patterns show LREE enrichment with chondrite normalized $(La/Yb)_N$ ratios ranging from 4.2–21.8 and $(La/Sm)_N$ ratios are between 3.9 and 7.2 (Fig. 9). The samples also have strong negative Eu-anomalies (Eu/Eu*=0.10–0.37). The primitive mantle normalized plots (Fig. 10) show distinct negative anomalies of Ba, Ta, Nb, Sr and Ti and positive anomalies of Th and U.

The Ailanghe granites have negative $\varepsilon Nd_{(T)}$ ratios of −5.7 to −6.7 and a large range of $_{I}Sr$ (0.7006 to 0.7110) which are likely meaningless. The Nd results are consistent with isotopic data ($\varepsilon Nd_{(T)}$=−6.3 to −6.2) reported by Zhong et al. (2007) for the same pluton.

6. Discussion

6.1. Duration of ELIP magmatism

The age of the ELIP is generally considered to be ~260 Ma as constrained by SHRIMP zircon U–Pb dating of mafic intrusions and some felsic plutons (Zhou et al., 2002b; Fan et al., 2004; Guo et al., 2004; Shellnutt and Zhou, 2006a). The age date of 260±2 Ma presented for the Woshui pluton is consistent with results for layered mafic intrusions and felsic plutons from the Panxi region. A SHRIMP zircon U–Pb age of 261±4 Ma date obtained by Zhong et al. (2007) for the Cida syenitic intrusion to the north of the Baima igneous complex is also contemporaneous with the 260 Ma emplacement age of the ELIP. The Panzhihua pluton is the only one which has not been dated, but the geological relationships constrain it to the late Permian because it has intruded the lower most lava flows of the Emeishan flood basalts and is overlain by the Early Triassic Bingnan Formation, a continental conglomerate unit. This, coupled with the fact that it is spatially associated with a ~260 Ma layered ore-bearing intrusions, like others (e.g., Hongge, Taihe, and Baima), strongly suggests that it is late Permian (Zhou et al., 2005).

The exact emplacement age of the ELIP remains somewhat controversial due to the 251–253 Ma Ar–Ar dating results of flood basalts from Lo et al. (2002). Ali et al. (2004) claim that the young ages produced from Ar–Ar dating may have been a result of post-emplacement tectonism affecting the region at various time intervals from the Mesozoic to the Cenozoic. Although the majority of age dates for the Panxi intrusions are ~260 Ma, there have been a few age dates reported at ~252 Ma from plutonic rocks. Using SHRIMP zircon U–Pb dating techniques, Shellnutt and Zhou (2006b) and Zhong et al. (2007) have dated the Huangcao syenite and the Ailanghe granite at 252± 2.5 Ma and 251±6 Ma, respectively. There is little doubt that the Huangcao syenite is a member of the ELIP and that ELIP magmatism extended from the middle Permian to the late Permian (Shellnutt and Zhou, 2006b). The younger age dates at ~252 Ma do not necessarily support the emplacement age of the Emeishan flood basalts because many of the 260 Ma plutonic rocks in the Panxi region have intruded the lower most flows. These dates do indicate that a minor pulse of ELIP magmatism occurred fairly late in its history producing a bimodal distribution of ages. Perhaps the most intriguing questions regarding the 252 Ma ages are: why was there a second melting period? and how did it occur? It is likely that the second melting event occurred during lithospheric extension associated with either post-emplacement relaxation of the Yangtze crust or external plate stress such as the South China–Indochina collision or South China–North China collision.

6.2. Petrogenesis of the Panxi felsic plutons

A-type granitic magmas are produced either by partial melting or fractional crystallization of mantle-derived mafic rocks or by partial melting of crustal rocks, although Bonin (in press) claims that no experimental A-type granitic liquids have been produced by crustal materials and that A-type granites are likely to be derived from transitional to alkaline mafic mantle sources (Collins et al., 1982; Clemens et al., 1986; Whalen et al., 1987; Eby, 1990, 1992; Frost and Frost, 1997; Smith et al., 1999). Mantle derived magmas may also assimilate crustal material during their ascent or residency time in the crust to produce 'mixed' source characteristics (Poitrasson et al., 1995).

The Panzhihua, Taihe and Woshui plutons have positive $\varepsilon Nd_{(T)}$ values (+1.5−+3.1) and do not show negative Ta–Nb anomalies (Figs. 8 and 10). The $_{I}Sr$ ratios for the peralkaline rocks are not likely to be meaningful because the results are unreliable when corrected to their radiometric age. On the other hand the samples from the Woshui pluton, corrected to 260 Ma, show a narrow range (0.7043–0.7044), consistent with mafic rocks in the region. In any case, these granites have $\varepsilon Nd_{(T)}$ values of mantle derived origin and plot in the field of within-plate (anorogenic) granitic rocks (Pearce et al., 1984; Batchelor and Bowden, 1985).

The Ailanghe granites have a different source. Their negative $\varepsilon Nd_{(T)}$ values (−5.7 to −6.7) and prominent negative Ta–Nb anomalies suggest derivation from a crustal source (Fig. 10). Their isotopes also suggest that the granites may have formed by crustal melting associated with the arrival of the ELIP plume head at the base of the crust. There is a problem however, the Ailanghe pluton is ~9 Ma younger than the onset of ELIP magmatism. So, why did it take so long for the crust to melt if a mantle plume could cause anatexis?

6.2.1. Peralkaline plutons

Geologically, these plutons are all stratigraphically above the layered intrusions and show conjugate trace

element relationships (Figs. 9 and 10). It is interesting to note that the associated mafic intrusions (e.g. Panzhihua, Baima and Taihe) contain oxide deposits in the lower third of the intrusions; typically magmatic oxide deposits are located in the upper third of intrusions for example the Bushveld (Lee et al., 1996). The peralkaline granitic rocks are spatially, temporally and chemically related to the layered intrusions and are likely associated with the formation of the Fe-Ti-V oxide deposits (Chen, 1990; Yang et al., 1997; Shellnutt and Zhou, 2006a). The exact process which connects the two rock types is unknown, however the presence of an oxide deposit and the mafic-felsic association without intermediate compositions, suggest that they may be related to either magma unmixing or fractional crystallization. There are problems with fractional crystallization most notably the mass-balance issue between the mafic and felsic rocks. Fractionation of mafic magmas will produce a small amount of felsic magma (Peccerillo et al., 2003). It is clear that relative proportions of the mafic and felsic rocks of the Panxi region is not in agreement with mass-balance and suggests fractionation may not be the process responsible or that there is an unseen mafic-ultramafic portion underneath the intrusion. If fractionation of the mafic magmas produced the peralkaline magmas it is likely that the enrichment of metals occurred after the segregation of the two magma types. This would require effective separation of the two magmas without intermediate compositions and oxygen enrichment to allow for the massive crystallization of oxide minerals. The spatial, temporal and geological evidence strongly suggests that the formation of these plutons with the layered mafic intrusions is not a coincidence and that a regional scale process occurred. It is likely that some mafic magmas from the ELIP mantle plume source were emplaced near the surface and differentiated (e.g. convective fractionation) producing the layered mafic intrusions and peralkaline plutons at the same time (c.f. Turner and Campbell, 1986).

6.2.2. Metaluminous plutons

Although the syenites from the Huangcao and Woshui plutons are spatially related, they are mineralogically and temporally different from each other. The Huangcao pluton is ~8 Ma younger than the Woshui pluton and contains fayalite, quartz and ferroan augite. Even though their mineralogies are different, they share similar major and trace element chemistry (Figs. 7–10). The chondrite normalized REE patterns are parallel and show the same positive Eu-anomalies. The patterns from the Woshui pluton are 200–400 times more than chrondrite values while the Huangcao syenite patterns are generally between 60–100 times chondrite values (Fig. 9). The primitive mantle (PM) normalized trace element plots show similar patterns and have the same concentration differences as the REE (e.g. the Woshui syenite is 200–400 times PM values).

The Woshui syenites have major element trends which may indicate fractionation of source already depleted in Th–U and Hf–Zr. Typically, A-type granites contain low amounts of Ba and Eu and high concentrations of Zr (Loiselle and Wones, 1979). The fact that the metaluminous plutons have high Ba and Eu, and low Zr suggests 1) they contain cumulate alkali feldspar and 2) they did not originate from the same magmas as the peralkaline plutons.

The positive Eu-anomalies indicate the granites originated from a source rock which either had abundant Eu or already experienced melting (Scoates et al., 1996). Cumulate plagioclase is typically the reservoir for Eu in mafic-ultramafic intrusions (e.g., BIC) and, as a result, any magma derived from partial melting or fractionation will be depleted in Eu. If the cumulate rocks melted again, the melts could be Eu-enriched. The Th–U and Hf–Zr negative anomalies are also indicative of partial melting from a depleted source, possibly a mafic magma which has already undergone partial melting, because these elements tend to be compatible in felsic rocks due to the crystallization of zircon, baddelyite or titanite. Shellnutt and Zhou (2006b) have suggested the Huangcao syenites formed by partial melting of rocks from the underplated mafic magmas. They suggest that mafic magmas injected into the lower crust of the Yangtze Block at ~260 Ma were the source for some of the flood basalts and mafic-felsic composite intrusions. Rocks from these magmas melted again at 252 Ma to produce the Huangcao syenite and the depleted Th–U and Hf–Zr compositions. We suggest this model may be appropriate for the formation of the Woshui pluton. There is a problem however with respect to the ages. The Woshui pluton is 8 m.y. older than the Huangcao syenite. As a modification to the partial melting model of Shellnutt and Zhou (2006b), we suggest that the Woshui pluton was derived by partial melting of the underplated mafic magmas shortly after extraction of first melts which produced the flood basalts. Because of the spatial and geochemical (e.g. high K_2O in the Huangcao syenite) relationships between the Huangcao syenite and the Woshui syenite, we suggest that the Huangcao syenites formed by melting of similar source material as the Woshui syenites. Derivation from the same source material could explain the Fe-enrichment, REE patterns, trace element normalized plots, spatial relationship and isotopic compositions of the Woshui and Huangcao syenites.

6.2.3. Peraluminous pluton

The relationship between the Ailanghe pluton and the other plutons in this study is problematic. Its status as an A-type granite may be debated (Zhong et al., 2007) but it has most of the features associated with the definition of A-type granites by Loiselle and Wones (1979) and Frost et al. (2001). In fact the Ailanghe granites are similar in composition and mineralogy to the peraluminous A-type granites of Australia (Turner et al., 1992; King et al., 1997). Rocks similar to the Ailanghe granites are also thought to be derived by melting of crustal sources but are considered I-type (Roberts and Clemens, 1992). The chemistry of course is supplementary to the fact that the geological setting is within plate and not associated with a collisional event or melting of sedimentary rocks (e.g. no muscovite or alumino-silicates). However, the most abundant mafic mineral is hornblende and the bulk composition does overlap with I-type granites but they have >1% normative corundum and >1.1 ANKC (Chappell and White, 1974). To add more uncertainty, the Ailanghe granite has a low Ga/Al ratio falling within the I-type classification field of Whalen et al. (1987) but falls within the within-plate granite field of Pearce et al. (1984). Also, the Ailanghe granite has lower concentrations of Zr, Y and Zn than other peraluminous A-type granites (King et al., 1997).

The isotopic and trace element signatures indicate that the Ailanghe granites formed by crustal melting and was emplaced at 251±6 Ma (Zhong et al., 2007), similar to the age of the Huangcao syenite (Figs. 10 and 11). This age is within the range of published dates for the ELIP. However, some problems arise because 1) it formed late in ELIP history and 2) there is a large error (±6 Ma) associated with the age date.

The arrival of a mantle plume head at the base of the crust is thought to be one cause for melting of crustal rocks (White and McKenzie, 1989; Campbell and Griffiths, 1990; Hill, 1993; White and McKenzie, 1995). In fact some mantle plume derived LIPs have silicic magmas erupt first followed by ultramafic and mafic lavas. These early silicic lavas are thought to represent crustal melts just before the eruption of the mantle derived lavas (Campbell and Hill, 1988; Hill et al., 1992; Hill, 1993). If crustal melts are amongst the first lavas to erupt then why is the Ailanghe granite melting ~9 Ma after the eruption and emplacement of ELIP lavas and plutons? Campbell and Hill (1988) suggest that differences between heat conduction of the mantle and crust may be one reason for the delay in melting of crustal material. This delayed melting event may explain the formation of the Ailanghe granites. However, it does not explain the formation of the contemporaneous Huangcao syenites because rocks of this composition require temperatures between 800 and 950 °C (Young and Cuthbertson, 1994). Huppert and Sparks (1988) suggest temperatures of ~900–950 °C could be obtained by injecting basaltic magmas into the crust and cause melting near the magma/crust boundary. The problem is that ELIP magmatism was short lived (<1 m.y.) and injection of basaltic magmas stopped around 258 Ma (Huang and Opdyke, 1998; Thompson et al., 2001; Guo et al., 2004). So if there was a delay in heat conduction between the plume and crust, why would the Huangcao syenite still be ~800–950 °C when it, being mantle derived, would have cooled at a rate different than from the crust and still be at it's liquidus temperature 9 Ma after magmatism stopped? Also the comparative volumes of material dated at ~260 Ma and ~252 Ma are greatly in favor of the older material. Because the younger magmatism is not widespread, melting of these rocks was likely caused by other factors. There are only a few possibilities which could explain the younger magmatism however they all must occur during extension of the Yangtze crust and after the doming stage of ELIP and eruption of the Emeishan flood basalts.

He et al. (2003) have provided strong sedimentological evidence for crustal doming in the vicinity of the Panxi region. They suggest that crustal doming occurred in the region prior to the eruption of the Emeishan flood basalts and ended by the beginning of the late Permian centered on the Panxi region. Evidence of doming is important support for the mantle plume hypothesis (Coffin and Eldholm, 1994; He et al., 2003; Xu et al., 2004). We suggest that post-emplacement extension of the ELIP dome may have caused a minor decompressional melting event at ~252 Ma and could be responsible for the formation of the Ailanghe pluton and likely the Huangcao pluton. Alternatively, it is possible that Permo–Triassic (250–240 Ma) back-arc extension of the South China Block during collision with the Indochina Block may have caused crustal extension in the Yangtze Block which melted the crust to the produce the Ailanghe granites (Lepvrier et al., 2004). Some large ion lithophile element-high field strength element ratios (e.g. Rb/Nb, Th/Ta, La/Ta, Rb/Zr) can be used as indicators for crustal reservoirs. It is thought that these ratios are preserved or are enriched in the melts produced from anatexis. The LILE/HFSE overlap between the Neoproterozoic granites and Permian Ailanghe granites (Fig. 11) suggests crustal derivation of the Ailanghe granites, possibly from the same reservoir (e.g. Yangtze basement). Finally the T_{DM} calculated dates for the Ailanghe granites are 1860 Ma, 1380 Ma and 1330 Ma respectively which also supports a Yangtze basement source.

Throughout Eurasia there are examples of silici-clastic volcanic layers at or near the Permo–Triassic (~251 Ma) boundary especially in South China (Yin et al., 1992). The Ailanghe and Huangcao plutons are contemporaneous with this volcanism. At this point there is no conclusive evidence as to why there was Permo–Triassic magmatism in this region only that there was Permo–Triassic magmatism.

6.3. Emplacement model for Permian Panxi felsic plutons

The emplacement of all the Permian Panxi granites may be explained by a mantle plume. The granitic intrusions discussed in this paper are directly or indirectly related to melting of a mantle plume source. A simplified model involving two stages of magmatism is thus proposed to explain the distribution and duration of Permian plutonism in the Panxi region.

Prior to ELIP magmatism the Yangtze Block was covered by shallow marine carbonates of the Maokou Formation (Fig. 12). The arrival of the Emeishan mantle plume causes uplift and doming of the Yangtze Block over a radius of 800 km centered near the Panxi region at ~260 Ma (Fig. 12). He et al. (2003) suggest that the uplift was rapid and ended around 258 Ma. During this stage mafic magmas were emplaced into the crust and produced the Emeishan flood basalts and intrusive rocks (Xu et al., 2004). Some mafic magmas differentiated to form the layered mafic intrusions and their associated peralkaline granitic rocks (Fig. 12). Differentiation and oxidization of the mafic magmas likely formed the peralkaline felsic magmas and enriched the mafic magmas in Fe-Ti-V from which the giant magmatic Fe-Ti-V oxide deposits formed. The conditions for the formation of the Fe-Ti-V deposits are likely consistent throughout the Panxi region due to the presence of at least three similar types of deposits. Immediately following the eruption of the Emeishan lavas, continued melting of the underplated mafic cumulate rocks produced the Woshui pluton. It is likely that other plutons in this region formed in a similar manner and assimilated crustal material during their ascent, for example the Cida granite (Zhong et al., 2007).

After the main effusive and plutonic period of ELIP magmatism, a second period of magmatism occurred at ~252 Ma and produced the Huangcao and Ailanghe plutons (Fig. 12). This volumetrically minor plutonism could be related to decompressional melting of the underplated mafic magmas and Yangtze basement rocks. The cause of the melting is currently unknown but collapse of the ELIP dome or Permo–Triassic (250–240 Ma) back-arc extension may have caused the second melting event. Currently there is no definitive evidence which explains the second melting event.

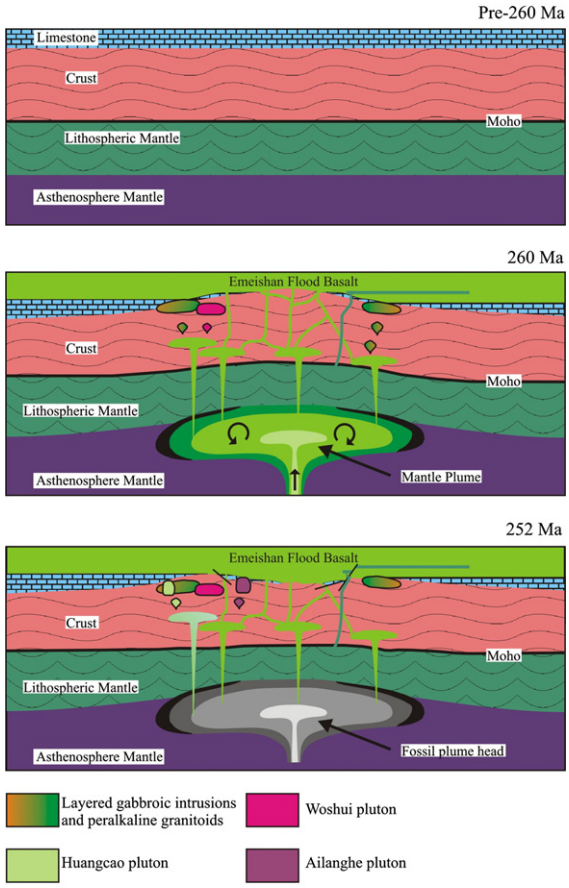

Fig. 12. Three stage model of the petrogenesis of the Panxi granites. Pre-260 Yangtze Block is covered by the Maokou formation. At 260 Ma the ELIP plume head arrives at the base of the lithosphere causing domal uplift of the crust and decompressional melting of the plume source. The melting injected mafic magmas in the lower crust/upper mantle, producing the Emeishan flood basalts and Fe-Ti-V bearing layered gabbroic intrusions. The layered mafic magmas differentiated to produce the peralkaline syenites. Fractional crystallization of the mafic underplated magmas produced the Woshui syenite contemporaneous with the main period of magmatism. Remelting of the underplated mafic magmas occurred to produce the highly evolved fayalite syenite at 252 Ma. Concurrent melting of the Yangtze basement produced the Ailanghe granite.

6.4. Implications for the formation of A-type granitic rocks

The specific and yet 'ambiguous' definition of A-type granitoids (Loiselle and Wones, 1979) manages to cause much debate as to what the 'A-' should stand for (e.g. anorogenic, alkaline, anhydrous, ambiguous). It is clear, as shown in this paper and others, that the formation of peralkaline, peraluminous and metaluminous A-type granitoids are mutually exclusive and formed by vastly different processes and yet they may all be geologically related (Collins et al., 1982; Anderson and Thomas, 1985; Sylvester, 1989; Nyman et al., 1994). Frost et al.

(2001) have suggested an alternative granite classification scheme which minimizes the ambiguity associated not only with A-type granites but I- and S-types as well.

The Panxi region contains three types of A-type granites. The formation of the ferroan peralkaline and metaluminous granites originated from melting of mantle-derived rocks. The peralkaline granites are differentiation products of the layered gabbroic intrusions and the metaluminous likely formed by remelting of underplated cumulate magmas. This is contrasted with the formation of the ferroan calc-alkalic peraluminous granite which likely form by melting of the Yangtze Block basement rocks.

7. Conclusions

In the Panxi region, SW China, peralkaline, peraluminous and metaluminous A-type granitic rocks are members of the ELIP. The peralkaline granites are spatially and temporally associated with oxide ore bearing layered gabbroic intrusions and were emplaced at ~260 Ma. The metaluminous granites were likely derived from melting of mafic cumulate rocks from the underplated ELIP magmas and were emplaced at ~252 Ma and ~260 Ma, respectively. Both the peralkaline and metaluminous granites were thus mantle-derived. The peraluminous granite was emplaced at ~251 Ma and was likely formed by partial melting of Yangtze basement rocks. The discrepancy between the older ages (~260 Ma) and younger ages (~252 Ma) suggests there were two stages of melting in the Panxi region. The first stage was directly related to the melting of the ELIP mantle plume head and the second occurred 8–9 m.y. later. This study suggests that a variety of A-type granitoids may occur in a similar geological setting.

Acknowledgements

The authors would like to thank Professor Ma Yuxiao and Mr. Zhao Hao from Chengdu University of Science and Technology for their field support and Mr. Liang Qi, Jianfeng Gao and Ms. Xiao Fu for their analytical support at the University of Hong Kong. This study is supported by grants from the Research Grant Council of Hong Kong, SAR (HKU7057/05P) and Chinese Academy of Science (2005-2-21).

References

Ali, J.R., Thompson, G.M., Zhou, M.-F., Song, X.Y., 2004. Emeishan basalt Ar-Ar overprint ages define several tectonic events that affected the western Yangtze platform in the Mesozoic Cenozoic. Journal of Asian Earth Science 23, 163–178.

Anderson, J.L., Thomas, W.M., 1985. Proterozoic anorogenic two-mica granites: Silver Plume and St. Vrain batholiths of Colorado. Geology 13, 177–180.

Anderson, I.C., Frost, C.D., Frost, B.R., 2003. Petrogenesis of the Red mountain pluton Laramie anorthosite complex: implications for the origin of A-type granite. Precambrian Research 124, 243–267.

Batchelor, R.A., Bowden, P., 1985. Petrogenetic interpretation of granitoid rock series using multicationic parameters. Chemical Geology 48, 43–55.

Black, L.P., Kamo, S.L., Allen, C.M., Aleinikoff, J.N., Davis, D.W., Korsch, R.J., Foudoulis, C., 2003a. TEMORA 1: a new zircon standard for Phanerozoic U–Pb geochronology. Chemical Geology 200, 155–170.

Black, L.P., Kamo, S.L., Williams, I.S., Mundil, R., Davis, D.W., Korsch, R.J., Foudoulis, C., 2003b. The application of SHRIMP to Phanerozoic geochronology; a critical appraisal of four zircon standards. Chemical Geology 200, 171–188.

Bonin, B., in press. A-type granites and related rocks: evolution of a concept, problems and prospects. Lithos.

Bruguier, O., Lancelot, J.R., Malavieille, J., 1997. U–Pb dating on single detrital zircon grains from the Triassic Songpan-Ganze flysch Central China: provenance and tectonic correlations. Earth and Planetary Science Letters 152, 217–231.

Campbell, I.H., Griffiths, R.W., 1990. Implications of mantle plume structure for the evolution of flood basalts. Earth and Planetary Science Letters 99, 79–93.

Campbell, I.H., Hill, R.I., 1988. A two-stage model for the formation of the granite-greenstone terrains of the Kalgoorlie–Norseman area, Western Australia. Earth and Planetary Science Letters 90, 11–25.

Chappell, B.W., White, A.J.R., 1974. Two contrasting granite types. Pacific Geology 8, 173–174.

Clemens, J.D., Holloway, J.R., White, A.J.R., 1986. Origin of an A-type granite: experimental constraints. American Mineralogist 71, 317–324.

Chen, F., 1990. Petrologic study on the Baima ore-bearing layered mafic-ultramafic intrusion. Acta Petrologica Sinica 4, 12–25 (in Chinese).

Chen, F., Hegner, E., Todt, W., 2000. Zircon ages, Nd isotopic and chemical compositions of orthogneisses from the Black Forest, Germany — evidence for a Cambrian magmatic arc. International Journal of Earth Science 88, 791–802.

Chen, F., Siebel, W., Satir, M., Terzioglu, N., Saka, K., 2002. Geochronology of the Karadere basement (NW Turkey) and implications for the geological evolution of the Istanbul zone. International Journal of Earth Science 91, 469–481.

Chung, S.L., Jahn, B.-M., 1995. Plume-lithosphere interaction in generation of the Emeishan flood basalts at the Permian–Triassic boundary. Geology 23, 889–892.

Chung, S.L., Jahn, B.-M., Genyao, W., Lo, C.H., Bolin, C., 1998. The Emeishan flood basalt in SW China: a mantle plume initiation model and its connection with continental breakup and mass extinction at the Permian–Triassic boundary. In: Flower, M.F.J., Chung, S.-L., Lo, C.H., Lee, T.Y. (Eds.), Mantle Dynamics and Plate Interactions in East Asia. American Geophysical Union Geodynamic Series, vol. 27, pp. 47–58.

Claoue-Long, J.C., Compston, W., Roberts, J., Fanning, M., 1995. Two Carboniferous ages: a comparison of SHRIMP zircon dating with conventional zircon ages and $^{40}Ar/^{39}Ar$ analysis. Geochronology Time Scales and Global Stratigraphic Correlation. SEPM Special Publication, vol. 54, pp. 3–21.

Coffin, M.F., Eldholm, O., 1994. Large igneous provinces: crustal structure, dimensions and external consequences. Reviews of Geophysics 32, 1–36.

Collins, W.J., Beams, S.D., White, A.J.R., Chappell, B.W., 1982. Nature and origin of A-type granites with particular reference to southeastern Australia. Contributions to Mineralogy and Petrology 80, 189–200.

Compston, W., Williams, I.S., Meyer, C., 1984. U–Pb geochronology of zircons from Lunar breccia 73217 using a sensitive high mass-resolution ion microprobe. Journal of Geophysical Research 89, 525–534.

Creaser, R.A., Price, R.C., Wormald, R.J., 1991. A-type granites revisited: assessment of a residual-source model. Geology 19, 163–166.

Eby, G.N., 1990. The A-type granitoids: a review of their occurrence and chemical characteristics and speculations on their petrogenesis. Lithos 26, 115–134.

Eby, G.N., 1992. Chemical subdivisions of the A-type granitoids: petrogenetic and tectonic implications. Geology 20, 641–644.

Fan, W., Wang, V., Peng, T., Miao, L., Guo, F., 2004. Ar–Ar and U–Pb geochronology of late Paleozoic basalts in western Guangxi and its constraints on the eruption age of Emeishan basalt magmatism. Chinese Science Bulletin 49, 2318–2327.

Frost, C.D., Frost, B.R., 1997. Reduced rapakivi-type granites: the tholeiite connection. Geology 25, 647–650.

Frost, B.R., Barnes, C.G., Collins, W.J., Arculus, R.J., Ellis, D.J., Frost, C.D., 2001. A geochemical classification for granitic rocks. Journal of Petrology 42, 2033–2048.

Guo, F., Fan, W., Wang, Y., Li, C., 2004. When did the Emeishan mantle plume activity start? Geochronological and geochemical evidence from ultramafic-mafic dikes in southwestern China. International Geology Review 46, 226–234.

He, B., Xu, Y.-G., Chung, S.-L., Xiao, L., Wang, Y., 2003. Sedimentary evidence for a rapid, kilometer-scale crustal doming prior to the eruption of the Emeishan flood basalts. Earth and Planetary Science Letters 213, 391–405.

Hill, R.I., 1993. Mantle plumes and continental tectonics. Lithos 30, 193–206.

Hill, R.I., Campbell, I.H., Davies, G.F., Griffiths, R.W., 1992. Mantle plumes and continental tectonics. Science 256, 186–193.

Hogan, J.P., Gilbert, M.C., Weaver, B.L., 1992. A-type granites and rhyolites: is A for ambiguous? Eos, Transactions of the American Geophysical Union 73, 447–457.

Huang, K., Opdyke, N.D., 1998. Magnetostratigraphic investigations of an Emeishan basalt section in western Guizhou Province, China. Earth and Planetary Science Letters 163, 1–14.

Huppert, H.E., Sparks, S.J., 1988. The generation of granitic magmas by intrusion of basalt into the crust. Journal of Petrology 29, 599–624.

King, P.L., White, A.J.R., Chappell, B.W., Allen, C.M., 1997. Characterization and origin of aluminous A-type granites from the Lachlan fold belt, southeastern Australia. Journal of Petrology 38, 371–391.

Landenberger, B., Collins, W.J., 1996. Derivation of A-type granites from a dehydrated charnockitic lower crust: evidence from the Chaelundi Complex, eastern Australia. Journal of Petrology 37, 145–170.

Lee, Eales, H.V., Cawthorn, R.G., 1996. A review of Mineralization in the Bushveld complex and some other layered mafic intrusions. In: Cawthorn, R.G. (Ed.), Layered Intrusions. Amsterdam, Elsevier, pp. 103–145.

LeMaitre, R.W., Bateman, P., Dudek, A., Keller, J., Lameyre, J., Le Bas, M.J., Sabine, P.A., Schmid, R., Sorensen, H., Streckeisen, A., Woolley, A.R., Zanettin, B., 1989. A Classification of Igneous Rocks and Glossary of Terms. Blackwell Scientific Publications, Oxford. 193 pp.

Lepvrier, C., Maluski, H., Tich, V.V., Leyreloup, A., Thi, P.T., Vuong, N.V., 2004. The early Triassic Indosinian orogeny in Vietnam (Truong Son Belt and Kontum Massif); implications for the geodynamic evolution of Indochina. Tectonophysics 393, 87–118.

Li, Z.X., Li, X.H., Kinny, P.D., Wang, J., 1999. The break-up of Rodinia: did it start with a mantle plume beneath South China? Earth and Planetary Science Letters 173, 171–181.

Liu, D., Jian, P., Kröner, A., Xu, S., 2006. Dating of prograde metamorphic events deciphered from episodic zircon growth in rocks of the Dabie–Sulu UHP complex, China. Earth and Planetary Science Letters 250, 650–666.

Lo, C.H., Chung, S.-L., Lee, T.-Y., Wu, G., 2002. Age of the Emeishan flood magmatism and relations to Permian–Triassic boundary events. Earth and Planetary Science Letters 198, 449–458.

Loiselle, M.C., Wones, D.R., 1979. Characteristics and origin of anorogenic granites. Geological Society of America Abstract with Programs 11, 468.

Long, L.E., Sial, A.N., Nekvasil, H., Borba, G.S., 1986. Origin of granite at Cabo de Santo Agostinho, northeast Brazil. Contributions to Mineralogy and Petrology 92, 341–350.

Ludwig, K.R., 2001. Isoplot/Ex, rev. 2.49: A Geochronological Toolkit for Microsoft Excel. Berkeley Geochronological Center, Special Publication, vol. 1a. 58 pp.

Luo, Z.-Y., Xu, Y.-G., He, B., Huang, X.-L., Shi, Y.R., 2006. A-type granite and syenite intrusions in Emeishan large igneous provinces: product of the Emeishan plume? International Conference on Continental Volcanism IAVCEI2006 Abstracts & Program, p. 63.

Ma, Y.X., Zhou, R.S., Wan, Y.W., Liu, F., Qiu, Y.D., Wang, H.F., 1999. Geology of Panzhihua City area (Map G-47-60-A). Chengdu University of Science and Technology, 1: 50000.

Maniar, P.D., Piccoli, P.M., 1989. Tectonic discrimination of granitoids. Geological Society of America Bulletin 101, 635–643.

Miller, C.F., 1985. Are strongly peraluminous magmas derived from pelitic sedimentary sources. Journal of Geology 93, 673–689.

Nyman, M.W., Karlstrom, K.E., Kirby, E., Graubard, C.M., 1994. Mesoproterozoic contractional orogeny in western North America: evidence from ca. 1.4 Ga plutons. Geology 22, 901–904.

Pearce, J.A., Harris, N.B., Tindle, A.G., 1984. Trace element discrimination diagrams for the tectonic interpretation of granitic rocks. Journal of Petrology 25, 956–983.

Pearce, J.A., 1996. Sources and settings of granitic rocks. Episodes 19, 120–125.

Peccerillo, A., Barberio, M.R., Yirgu, G., Ayalew, D., Maraieri, M., Wu, T.U., 2003. Relationships between mafic and peralkaline silicic magmatism in continental rift settings: a petrological, geochemical and isotopic study of the Gedemsa volcano, Central Ethiopian Rift. Journal of Petrology 44, 2003–2032.

Pitcher, W.S., 1997. The Nature and Origin of Granite. Chapman and Hall, London.

Poitrasson, F., Duthou, J.-L., Pin, C., 1995. The relationship between petrology and Nd isotopes as evidence for contrasting anorogenic granite genesis: example of the Corsican Province. Journal of Petrology 36, 1251–1274.

Potts, P.J., Thompson, M., Kane, J.S., Petrov, L.L., 2000. GEOPT7 — An International Proficiency Test for Analytical Geochemistry Laboratories. Report on Round, vol. 7. 35 pp., Unpublished report.

Potts, P.J., Thompson, M., Webb, P.C., Watson, J.S., 2001. GEOPT9 — An International Proficiency Test for Analytical Geochemistry Laboratories. Report on Round, vol. 9. 36 pp.

Qi, L., Jing, H., Gregoire, D.C., 2000. Determination of trace elements in granites by inductively coupled plasma mass spectrometry. Talanta 51, 507–513.

Roberts, M.P., Clemens, J.D., 1992. Origin of high-potassium, calc-alkaline, I-type granitoids. Geology 21, 825–828.

Song, X.-Y., Zhou, M.-F., Hou, Z.-Q., Cao, Z.-M., Wang, Y.-L., Li, Y., 2001. Geochemical constraints on the mantle source of the upper Permian Emeishan continental flood basalts, southwestern China. International Geology Review 43, 213–225.

Scoates, J.S., Frost, C.D., Mitchell, J.N., Lindsley, D.H., Frost, B.R., 1996. Residual-liquid origin for a monzonitic intrusion in a mid-Proterozoic anorthosite complex: the Sybille intrusion, Laramie anorthosite complex, Wyoming. Geological Society of America Bulletin 108, 1357–1371.

Smith, I.E.M., Johnson, R.W., 1981. Contrasting rhyolite suites in the late Cenozoic of Papua New Guinea. Journal of Geophysical Research 86, 10257–10272.

Sun, S.S., McDonough, W.F., 1989. Chemical and isotopic systematics of oceanic basalts: implications for mantle composition and processes. In: Saunders, A.D., Norry, M.J. (Eds.), Magmatism in the Ocean Basins. Geological Society of London Special Publication, vol. 42, pp. 313–435.

Shellnutt, J.G., Zhou, M.-F., 2006a. Enrichment of Fe, Ti, V in mafic magmas by immiscible separation of syenitic magmas: a case study of the Permian Baima igneous complex, Sichuan Province, SW China. International Conference on Continental Volcanism IAVCEI2006 Abstracts & Program, p. 181.

Shellnutt, J.G., Zhou, M.-F., 2006b. Rifting-related, Permian ferrosyenites in the Panxi region of the Emeishan large Igneous province, SW China. Geochimica et Cosmochimica Acta 70, 579.

Shellnutt, J.G., Zhou, M.-F., Qi, L., 2005. Major, Trace and platinum group elemental geochemistry of the Baima and Taihe magmatic Fe-Ti-V oxide deposits of the Permian (260 Ma) Emeishan large igneous province, SW China. GAC/MAC Joint Annual Meeting. Halifax, NS, Abstract, vol. 30, pp. 174–175.

Smith, D.R., Noblett, J., Wobus, R.A., Unruh, D., Douglass, J., Beane, R., Davis, C., Goldman, S., Kay, G., Gustavson, B., Saltoun, B., Stewart, J., 1999. Petrology and geochemistry of late stage intrusions of the A-type, mid-Proterozoic Pikes Peak batholith (Central Colorado, USA): implications for petrogenetic models. Precambrian Research 98, 271–305.

Sylvester, P.J., 1989. Post-collisional alkaline granites. Journal of Geology 97, 261–280.

Thompson, M., Potts, P.J., Kane, J.S., Wilson, S., 1999. GEOPT5 — An International Proficiency Test for Analytical Geochemistry Laboratories. Report on Round, vol. 5. 23 pp.

Thompson, G.M., Ali, J.R., Song, X.Y., Jolley, D.W., 2001. Emeishan basalts, southwest China: reappraisal of the formation's type area stratigraphy and a discussion of its significance as a large igneous province. Journal of the Geological Society of London 158, 593–599.

Turner, J.S., Campbell, I.H., 1986. Convection and mixing in magma chambers. Earth Sciences Reviews 23, 255–352.

Turner, S.P., Foden, J.D., Morrison, R.S., 1992. Derivation of some A-type magmas by fractionation of basaltic magma: an example from the Padthaway Ridge, south Australia. Lithos 28, 151–179.

Wan, Y., Wilde, S.A., Liu, D., Yang, C., Song, B., Yin, X., 2006. Further evidence for ~1.85 Ga metamorphism in the Central Zone of the North China Craton: SHRIMP U–Pb dating of zircon from metamorphic rocks in the Lushan area, Henan Province. Gondwana Research 9, 189–197.

Wang, D.R., Xie, Y.M., Hu, Y.J., You, X.X., Cao, J.X., 1993. Geology of Guogailiang area (Map G-48-1-A). Panxi Geological Team, Geology and Mineral Resources Bureau, Sichuan Province, 1: 50000.

Wang, D.R., Xie, Y.M., Wang, Q.J., Tao, Z.D., 1994. Geology of Guabang area (Map G-48-25-C). Panxi Geological Team, Geology and Mineral Resources Bureau, Sichuan Province, 1: 50000.

Whalen, J.B., Currie, K.L., Chappell, B.W., 1987. A-type granites: geochemical characteristics, discrimination and petrogenesis. Contributions to Mineralogy and Petrology 95, 407–419.

White, R.S., McKenzie, D., 1989. Magmatism at rift zones: the generation of volcanic continental margins and flood basalts. Journal of Geophysical Research 94, 7685–7729.

White, R.S., McKenzie, D., 1995. Mantle plumes and flood basalts. Journal of Geophysical Research 100, 543–585.

Xiong, X.Y., Xie, Y.M., Nie, K.H., Kan, Z.Z., Ding, L.R., Guo, J.Q., 1996. Geology of Miyi area (Map G-48-37-A). Panxi Geological Team, Geology and Mineral Resources Bureau, Sichuan Province, 1: 50000.

Xu, Y.G., Chung, S.L., Jahn, B.-M., Wu, G., 2001. Petrologic and geochemical constraints on the petrogenesis of Permian-Triassic Emeishan flood basalts in southwestern China. Lithos 58, 145–168.

Xu, Y.G., He, B., Chung, S.L., Menzies, M., Frey, F.A., 2004. Geologic, geochemical, and geophysical consequences of plume involvement in the Emeishan flood-basalt province. Geology 32, 917–920.

Yan, D.P., Zhou, M.-F., Song, H.L., Wang, X.W., Malpas, J., 2003. Origin and tectonic significance of a Mesozoic multi-layer overthrust system within the Yangtze Block (South China). Tectonophysics 361, 239–254.

Yang, R., Xu, W., Liu, R., 1997. REE geochemistry of Baima complex in the Panxi rift belt. Acta Mineralogica Sinca 17, 71–77 (in Chinese).

Yin, H., Huang, X., Zhang, K., Hansen, H.J., Yang, F., Ding, M., Bie, X., 1992. The effects of volcanism of the Permo–Triassic mass extinction in South China. In: Sweet, W.C., Yang, Z.Y., Dickins, J.M., Yin, H.F. (Eds.), Permo–Triassic Events in the Eastern Tethys: Stratigraphy, Classification, and Relations with the Western Tethys. World and Regional Geology, vol. 2, pp. 146–157.

Young, D.A., Cuthbertson, J., 1994. A new ferrosilite and Fe-pigeonite occurrence in the Reading Prong, New Jersey, USA. Lithos 31, 163–176.

Zhang, H.F., Sun, M., Lu, F.X., Zhou, X.H., Zhou, M.-F., Liu, Y.S., Zhang, G.H., 2001. Moderately depleted lithospheric mantle underneath the Yangtze Block: evidence from a garnet lherzolite xenolith in the Dahongshan kimberlite. Geochemical Journal 35, 315–331.

Zhong, H., Zhou, X.-H., Zhou, M.-F., Sun, M., Liu, B.-G., 2002. Platinum-group element geochemistry of the Hongge Fe-Ti-V deposit in the Pan-Xi area, southwestern China. Mineralium Deposita 27, 226–239.

Zhong, H., Zhum, W.-G., Song, X.-Y., He, D.-F., 2007. SHRIMP U–Pb zircon geochronology, geochemistry, and Nd–Sr isotopic study of contrasting granites in the Emeishan large igneous province, SW China. Chemical Geology 236, 112–133.

Zhou, M.-F., Yan, D.P., Kennedy, A.K., Li, Y., Ding, J., 2002a. SHRIMP U–Pb zircon geochronological and geochemical evidence for Neoproterozoic arc-magmatism along the western margin of the Yangtze block, South China. Earth and Planetary Science Letters 196, 51–67.

Zhou, M.-F., Malpas, J., Song, X.-Y., Robinson, P.T., Sun, M., Kennedy, A.K., Lesher, C.M., Keays, R.R., 2002b. A temporal link between the Emeishan large igneous province (SW China) and the end-Guadalupian mass extinction. Earth and Planetary Science Letters 196, 113–122.

Zhou, M.-F., Robinson, P.T., Lesher, C.M., Keays, R.R., Zhang, C.J., Malpas, J., 2005. Geochemistry, petrogenesis and metallogenesis of the Panzhihua gabbroic layered intrusion and associated Fe-Ti-V oxide deposits, Sichuan Province, SW China. Journal of Petrology 46, 2253–2280.